A review of Surface Matching models: perspectives and challenges for Automatic Soft-Tissue Registration in Computer-assisted Interventions

Thiago Ramos dos Santos[1]

Abstract

One of the main challenges related to Computer-Assisted Surgery (CAS) is the registration of multi-modal patient specific data to enhance the surgeon's navigation capabilities by observing beyond the exposed tissue surface. One increasingly popular approach involves capturing the organ surface with a range imaging device and performing a shape-based registration. This paper (1) discusses the major challenges related to surface matching in the operating theater and (2) provides a general review of state-of-the-art methods in shape matching.

Keywords: Intra-operative registration. Surface matching. Computer-assisted surgery.

***

1 Doutor, e-mail: thiago.ramos@sc.senai.br

***

0.1 INTRODUCTION

Due to their complexity and risks involved, many surgical procedures require extremely careful planning. Procedures such as the ablation of liver tumors, where a needle is used, which needs to be inserted directly in the center of the tumor in order to cauterize it from the inside to the outside, or liver resection, which consists of removing a part of the liver with the purpose of eliminating cancerous tissue, require very cautious consideration. In the case of tumor ablation, the needle must be inserted through several tissues including the skin of the patient in order to reach the tumor without harming any crucial organ, such as the lungs, or hitting solid structures, such as bones, which cannot be punctured. In the case of a liver resection, a part of the liver must be removed without damaging any vital arteries or veins and at the same time leaving enough organ volume behind to guarantee the physiological functions of the liver.

Surgical planning often involves the acquisition of three-dimensional (3D) medical images, such as computed tomographies (CT) or magnetic resonance imaging (MRI), which provide the surgeon with an overview of the patient's anatomy and potential pathologies. Given this information, the surgeon is able to identify a target structure, such as a tumor, and plan a path towards that target, along which a needle can safely be inserted. Alternatively, the surgeon can plan a cut to isolate a certain section of a partially dysfunctional organ, as is done during liver resection.

Unfortunately, a careful surgery plan does not always coincide with a successful surgery itself. Without assisting techniques, the implementation of the surgery plan is not trivial, as the patient's condition might change significantly from the moment when images used for planning are acquired to the moment when the surgery is performed: Among others, organ displacement, breathing, and heart beats, are some of the issues that must be dealt with during surgery. In this complex setting, the surgeon must still be able to adapt the surgery plan to the altered situation. Therefore, computer-assisted interventions are increasingly gaining significance in the surgical routine. Nowadays, several computer-based systems exist to assist surgeons in the real-time localization and visualization of organs, regions of interest and structures of risk, and to guide them towards target structures (see [1, 2, 3, 4, 5, 6, 7] for more extensive reviews on those systems).

Critical for surgery guidance is the computation of an alignment between the (virtual) space where the surgery planning was performed and the space where surgery is taking place. This task is called *registration*. Most existing commercial systems focus on assisting interventions near rigid structures, like bones, where they can rely on static anatomical landmarks or attach fiducial markers for the alignment of the spaces (*e.g.* BrainLab VectorVision).

In this scenario, the relative position between guidance landmarks does not

change and, assuming that the patient has been immobilized, registration between planning and surgery must only be performed once. However, researchers have drawn their attention to a more complicated problem: computer guidance for soft-tissue interventions. In contrast to rigid structures, soft tissues are continuously deformed due to respiratory motion, heart beats, and external forces (*e.g.* surgical manipulation). In this case, anatomical landmarks are usually not clear or not reliable due to deformations. Even if one resorts to fiducial markers as artificial landmarks, their position relative to each other is constantly changing.

> Computer-assisted guidance in soft-tissue interventions therefore remains very challenging.

Several authors have proposed the use of optically or magnetically tracked fiducial markers for the compensation of deformations during soft tissue interventions [8, 9, 10, 11, 12, 13, 14, 15, 16]. These fiducials are either placed above the skin or inside the organ of interest (needles), and are continuously tracked in order to determine their position. Deformation models are employed in order to estimate the location of the targets[1] based on the movement of the fiducials. The main drawback of the use of fiducial markers as surgical guidance aids is that the spatial configuration of the markers around the target is crucial for the minimization of target registration errors [17, 18, 19]. Markers placed above the skin are usually too far from the targets, being less reliable for target localization. While needles can be used for more reliable target localization, they are of a more invasive nature. After the attachment of the markers, 3D medical image acquisition must be repeated in order to establish the position of the anatomical structures in relation to the markers, exposing the patient to extra radiation, in the case of computed tomographies, for example. Furthermore, fiducial markers are not particularly suitable for open body surgery, as it would require the placement of the patient in a 3D image acquisition device with the body open and with the entire surgical apparatus. Nevertheless Weber et al. [20] and Markert et al. [21] presented some efforts for attaching markers on the liver surface. Maier-Hein et al. [22] investigated the optimal combination of skin markers and needles in order to maximize accuracy and minimize invasiveness. Image-based techniques have also been employed for guidance [23, 24, 25, 26, 27, 28, 29, 30]. These techniques usually involve the segmentation of organs, targets and instruments from real-time imaging modalities (*e.g.* ultrasound), or the direct image-to-image registration between pre- and intra-operative data. Image-guided techniques for the robust and accurate compensation of soft-tissue motion are still subject of ongoing research [31]. Imaging modalities such as ultrasound require direct body contact with the patient and are usually very noisy, while intra-operative X-ray and tomography devices (C-arms) expose the patient to additional radiation and require the isolation of the operation room during image acquisition. The combination of image-guided techniques with the use

[1]We denote as target any pre-defined point or region of interest whose position is to be found during surgery.

of fiducial markers has also been investigated [32, 33, 34, 35]. Here, the main task is the identification and extraction of the markers from the images, which constitutes a less complex problem than directly identifying organs, anatomical landmarks, and instruments.

Surface-based intra-operative registration is an attractive alternative for intra-operative guidance, as common surface scanners: (1) Do not require contact with the patient, thus also being suitable for open body surgery; (2) Do not expose the patient to radiation; (3) Do not require isolation of the operation room during acquisition; (4) Have moderate to high acquisition rates; and (5) Do not require any kind of markers. Having surface models from segmented pre-operative data, registration is obtained by matching intra-operatively acquired surfaces (*e.g.* surface of an organ or the skin) to pre-operatively acquired ones. As in the case of the use of fiducial markers, deformation models are required in order to correctly estimate the location of targets inside a particular volume based on the deformation of its surface. The use of surface matching techniques for intra-operative registration purposes is already being investigated [36, 37, 38, 39, 40, 41, 42, 43, 44, 45, 46, 47]. These authors have focused their attention to fine alignment algorithms, which are known to require an initial alignment in order to converge. They evaluated it for intra-operative purposes and proposed variations in order to make it more robust to initial alignments and to surface deformations. However, initial alignments are still performed manually or with the assistance of fiducial markers, in some cases requiring two sensors being placed in the operation room: one for surface acquisition and another for marker tracking. Manual alignments may be tedious and error prone, as they may be repeated several times during an intervention and the identification of landmarks is not always visually clear. Furthermore, in the case of laparoscopic interventions, manual alignments and marker placement are practically difficult, while the acquisition of surfaces using techniques such laserrange scanner or time-of-flight can be incorporated into laparoscopic or endoscopic devices [48].

So far, the automatic establishment of correspondences between pre- and intra-operatively acquired surfaces remains elusive, as surface matching in intra- operative settings poses a challenging problem. Numerous methods have been proposed for image registration in general [49, 50], and different imaging modalities, such as US, intraoperative CT and interventional MRI have been investigated for this purpose. However, these are often not well suited to real-time image acquisition in a surgical theatre with traditional instrumentation, provide poor image quality or are associated with radiation exposure and high costs. The focus of this paper is to provide the reader with a summary of the current state-of-the-art in surface matching techniques, relating them to the problem of establishing an alignment between pre- and intra--operatively acquired surfaces. We aim to identify technologies and new techniques that may be of use for surface-based intra-operative soft-tissue registration in the near future, pointing out the long term perspectives and challenges. Until

now, only Audette et al. [51] presented a related article, in the year 2000, which investigates surface registration techniques for medical imaging. However, this article is rather focused on the algorithmic basics of surface matching, and is not concerned about the issues that are relevant for surface matching in intra-operative environments. Furthermore, an entire decade has passed since its publication, since which, many improvements and innovations have occurred to the field.

This paper is organized as follows: First, we give a brief overview on surface- based intra-operative guidance systems and how they have been employed so far, also considering other stages in the pipeline that are not part of the surface matching procedure itself, and, therefore, outside of the scope of this paper (Sec. 0.2). Second, we outline the surface matching procedure and decompose it in its main stages (Sec. 0.3), presenting the state-of--the-art works for each stage and considering their suitability for intra-operative registration. Finally, we elaborate on the perspectives, limitations and challenges of surface-based intra-operative registration from a technical point-of-view (Sec. 0.4).

0.2 OVERVIEW OF SURFACE-BASED INTRA-OPERATIVE REGISTRATION

Registration refers to the process of transforming different data sets into one common coordinate system. During *intra-operative registration*, the coordinate system in which the intervention plan was specified is aligned to the reference coordinate system in the operation room. *Surface-based intra-operative registration* refers to the computation of a transformation that maps a pre-operative co- ordinate system, acquired by imaging techniques such as computed tomography (CT) or magnetic resonance imaging (MRI), to an intra-operative coordinate system, using the patient's current morphological (shape) information during surgery. Intra-operative registration is used to align and adapt structures, targets, trajectories, and other data previously generated during surgery planning to the patient's situation during surgery, in order to allow for adequate surgery guidance. The term surgery guidance refers to a way of communicating the current status of the surgery in relation to what was planned to the surgeon. In other words, this means showing information that helps the surgeon to follow the surgery plan. It may thus involve continuous intra--operative registration and tracking of surgical instruments. For more details on the history of surgical guidance and on the role of registration in the guidance process we kindly refer the reader to [52].

Procedures based on surface-based intra-operative registration are structured as follows (Fig. 1): Prior to the intervention, the patient is submitted to a volume scan, such as a CT or MRI, which generates a 3D image (volume). Given this volume, the physician is able to create different models for the different

objects (*e.g.* organs, vessels, tumors) by means of image segmentation algorithms (Sec. 0.2.1). These models are the basis for the generation of surfaces of interest, which will be used for the subsequent registration, but also for the construction of a intervention plan, which determines the course and goals of the surgery (*e.g.* a trajectory for needle insertion that avoids structures of risk, such as the lungs, or a liver resection that avoids injury of major arteries and vessels). Surgery plans are usually built with specialized software. Once surgery is about to start, the remaining task is the adaption of pre-operatively generated information to the patient's current situation. This implies a non-trivial problem, as the organ of interest deforms due to patient movements, breathing, or surgical manipulations. This task is accomplished by the acquisition of intra- operative data and by matching it to pre-operative data, in order to establish a spatial relation between the two. With regards to this work, the information used for registration is morphological data represented by surfaces.

Surfaces are acquired intra-operatively by means of range imaging devices (Sec. 1.2.2), which generate range images (also known as depth images) with each pixel representing a distance value. Range images are converted into surfaces by a sequence of pre-processing stages (Sec. 1.2.3), aiming at identifying the objects of interest and to compensate for possible image distortions and errors intrinsic to the image acquisition technology. The spatial relation between the pre- and intra-operative situations is established by means of surface matching, which is the main topic of this work, and is investigated in detail in Sec. 1.3. After a spatial relation is established, the surgery plan can be adapted to the patient's current situation for the purpose of guidance. This is achieved by means of a physics-based deformation model, which extrapolates the transformation obtained for the surfaces to the organ's entire volume.

Figura 1: Processing pipeline for surface-based intra-operative registration

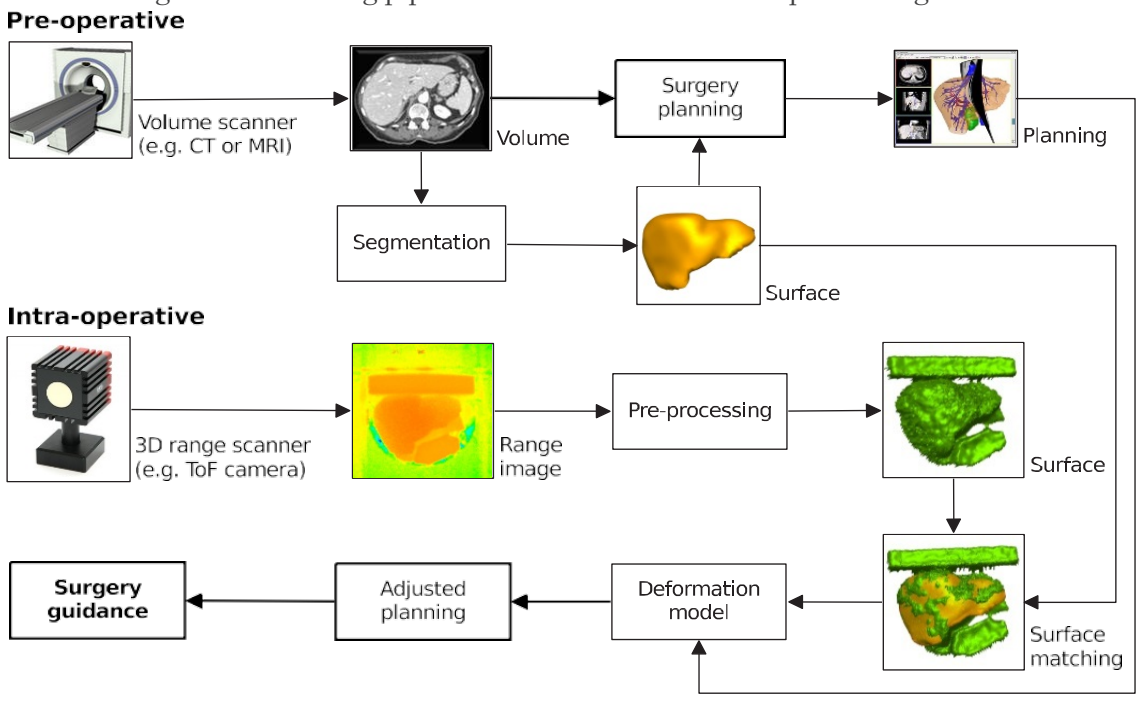

When designing a method for the automatic establishment of correspondences between pre- and intra-operatively acquired surfaces, the following issues must be taken into consideration, which turns surface matching for intra- operative registration purposes in a challenging and non-trivial problem, as it imposes several challenges:

1. **Partial surfaces:** As 3D scanners do not have a complete view of the region of interest, and there are also many other objects and structures in the environment, we must deal with a partially overlapping surfaces matching problem. Furthermore, due to the different acquisition principles, holes on one surface may not be present on the other one.
2. **Noise:** Depending on the acquisition rates, surfaces generated by 3D scanners can be noisy. Usually, the higher the acquisition rate, the higher the amount of noise on the surfaces.
3. **Distortions:** Due to the different acquisition principles of intra- and pre-operatively generated surfaces (multi-modality), and the different systematic errors that are inherent to these principles, distortions on local and global scales can occur.
4. **Non-rigidity:** As the organ of interest may be undergoing deformation due to respiratory motion or from the surgical intervention, the surface is subject to complex deformations. In this case, the spatial configuration of a set of points on one surface and the configuration of their corresponding ones on the other surface might be different.
5. **Lack of structure:** Usually, surfaces of interest do not present a clear structure or articulation (*e.g.* a clear subdivision of the human body into arms, legs and head) which could be used as reliable landmarks. Matching of surfaces with a clear subdivision into several parts poses a less complex problem, as it resumes to identifying these parts and establishing correspondences between them.
6. **Lack of landmarks:** Surfaces of interest for intra-operative registration often do not present prominent regions or locations, which could be used as reliable landmarks. Surfaces acquired intra-operatively are mostly nearly flat, such as the partial surface of a liver, for example.
7. **Speed:** The entire matching process must be completed in reasonable space of time, *i.e.*, ideally within a few seconds, although within a couple of minutes is acceptable.

Due to these issues, surface matching for intra-operative registration has been used so far only for accounting of displacements that occur in local scales, by means of variations of the *iterative closest point* (ICP) algorithm [36, 37, 38, 39, 40, 41, 42, 43, 44, 45], whereas the actual registration between the intra- and pre-operative spaces occurs manually. Several surface-based navigation systems for cranio-maxillo-facial surgery based on ICP already exist, which have been extensively evaluated in the clinical context [53, 54, 55, 56, 57].

In the following sections, we review the stages involved in surface-based intra-operative registration, highlighting relevant work on these topics.

0.2.1 Image segmentation

Image segmentation means the partitioning of an image into multiple segments, *i.e.*, the assignment of image pixels or voxels to different regions. These segments should make sense in the context of a particular application. In medical imaging, segmentation focuses on the identification of regions and boundaries of organs, tumors, and other anatomical structures, in order to enable the quantification of an organ's specific measurements (*e.g.* volume, blood irrigation, etc). Segmentation allows for the computation of surfaces representing the objects of interest. These surfaces can be used for the purpose of registration.

For more details on medical image segmentation methods, we refer the reader to [58, 59, 60].

0.2.2 Range imaging devices

Three-dimensional (3D) imaging systems (or range scanners) are devices that measure the distance between the device itself and the objects in its field-of-view. The result is usually an image, referred to as range or depth image, in which each pixel represents a distance value (Fig. 2b). The most widely used 3D imaging systems for surface data are *stereoscopic imaging* [61,62], *structured light* [63], and *laser range scanning* [64]. A very promising new technology for range scanning are *time-of-flight* (ToF) cameras [65, 66, 67], which are able to simultaneously generate a light intensity image and a range image at high acquisition frequency rates. However, the drawback of the ToF cameras are the systematic errors and potentially high noise levels.

Figura 2: Acquisition of the surface of an object by a time-of-flight (ToF) camera. (a) The object (a mug); (b) The acquired range image, with distance values mapped to a color palette ranging from green (further) to red (near); (c) Ex- traction of the object of interest; (d) Conversion of the range image into a 3D point cloud; (e) Triangulation of the point cloud in order to build a surface. For more comprehensive reviews on the topic of 3D range scanning please refer to [68, 69, 70]

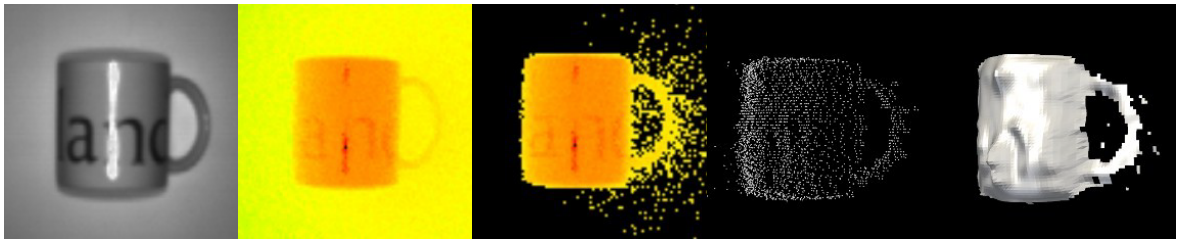

(a) (b) (c) (d) (e)

0.2.3 Range images to surfaces

Here, we present the required pre-processing steps for the conversion of a range image into a surface representation (polygonal mesh). As intra-operative

environments are usually filled with different objects, which may appear in the acquired range images, imposing extra complexity to the surface matching procedure, we present a brief overview of object recognition in range images in Sec. 1.2.3.1, which aims to isolate the object of interest (region or organ) from other objects. In Sec. 1.2.3.2 we describe the conversion of range data in a surface representation, focusing on triangle meshes, which are one of the most commonly used discrete representations for surfaces. Finally, Sec. 1.2.3.3 presents data structures for the representation of meshes. These data structures allow the efficient computation of mesh properties, which are required for surface matching.

0.2.3.1 Object recognition

Object recognition deals with the problem of identifying a particular object in an image. It has been subject of research for more than four decades [71]. Major problems in the field of object recognition, are the detection of objects from different camera points-of-view, lighting conditions and partial occlusion by other objects in the scene [72]. The different approaches for object recognition are usually classified as follows: *Geometry-based approaches* [72], which employ the geometric properties of the object of interest, and its projection on 2D planes; *Appearance-based approaches* [73], which attempt to capture the visual appearance of the object; and *Feature-based approaches* [74], which focus on finding points-of-interest that are used to characterize the desired object. Object recognition is closely related to image segmentation (see Sec. 1.2.1), and, in fact, many object recognition approaches employ certain segmentation techniques.

In the case of range images, the use of appearance-based approaches is somewhat limited, as the appearance of a particular object in the image varies according to its distance to the camera. However, some scanners, such as the time-of-flight camera, can simultaneously acquire a light intensity image, which.

Figura 3: Projection of an object in 3D space to the 2D space of an image according to the *pinhole camera model* can be used for appearance-based detection. Several authors have focused on the specific problem of detecting objects in range images, as can be found in [75,76,77]

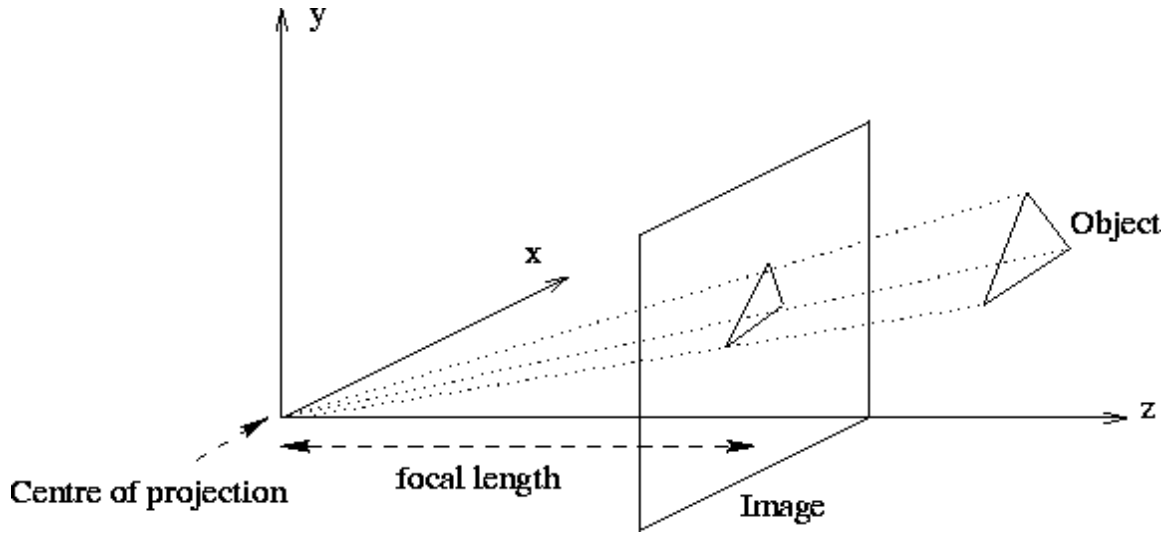

0.2.3.2 Surface generation

In order to construct a surface from a range image, the first step is to convert the image into a spatial representation: Each pixel in the range image is converted to a 3D point (Fig. 2d). This conversion is performed according to the *pinhole camera model* (Fig. 3), which allows the computation of the original 3D position of the object based on its projection onto the image plane [78]. Several image distortions may occur due to lens effects and measurement principles, which must be compensated for correct geometry computation [78, 79, 80]. The second step in the conversion process is the establishment of neighborhoods for each point, representing these neighborhoods by edges, in order to form meshes (Fig. 2e). Triangle meshes are the most widely employed discrete representation of surfaces, although meshes composed by other polygons are also possible [81]. Kilgus et al. [82] investigated and compared several alternatives for the generation of triangle meshes from point sets generated by ToF cameras.

0.2.2.3 Data structures for mesh representation

The representation of meshes using appropriate data structures is advantageous for several reasons, including the accelerated retrieval of adjacency and incidence information, the efficient object traversal, and the maintenance of topological consistency during manipulation. The use of efficient data structures may be critical for achieving the required performance in the case of surface matching, where the computation of neighborhoods and surface properties (*e.g.* curvatures) becomes necessary. Also desirable for a mesh representation data structure is the ability to represent the boundaries of the meshes, as objects scanned by range scanners have open boundaries. The detection and representation of mesh anomalies, such as *non-manifoldness*[2], is also crucial. Several descriptors require the surfaces to be a perfect manifold for their computation, and the detection of such anomalies is important so they can be treated and repaired in a pre-processing stage. Having a data structure that is able to efficiently detect and treat the afore mentioned anomalies is crucial for the efficiency and efficacy the surface matching algorithm.

Most widely employed data structures for mesh representation are the *winged- edge* [83, 84], the *quad-edge* [85] and the *doubly-linked face list* [86,87], for the representation of perfect manifolds. The *half-edge* representation [88] can also be used for representation of boundaries. More recently, dos Santos et al. [89] presented the *extended doubly-linked face list*, which allows for the representation of boundaries and some non-manifold cases very efficiently.

0.2.4 Deformation Models

Deformation models are employed to extrapolate deformation information on one part of the organ to the rest of its entire volume. These models are usually based on physically coherent models, such as the *finite element method* (FEM) [90], in

[2] A mesh is said to be a *manifold* if, for every point, the surface is locally equivalent to an open disk. If this is not the case, the mesh is said to be a *non-manifold*.

order to compute extrapolations that are plausible with the physical reality. Literature on deformation models can be found, for example, for the kidneys [91], the liver [38, 92] and the brain [93]. A model for the computation of internal abdominal motion based on the skin deformation was presented by Hostettler et al. [94].

0.3 SURFACE MATCHING

Surface matching is a large field and it has been studied for several years. The primary goal of surface matching is to compute a mapping from one surface onto another, and it can be regarded as an optimization problem. Because of the many existing approaches to matching surfaces, classifying them into meaningful groups is not trivial. Audette et al. [51] addressed this issue by first decomposing the surface matching procedure into its main stages, followed by classification of the methods according to how each stage was approached. Similar to Audette et al. [51], we also consider three different stages: *descriptor representation* (Sec. 1.3.1), *optimization* (Sec. 1.3.4) and *transformation* (Sec. 1.3.5). However, another component plays a major role in registration, and it is relevant to analyze it on its own: the *error metric* (Sec. 1.3.3), which is attempted to be minimized during optimization. Another important stage, commonly used in surface matching for reducing the search-space and increasing the chances of finding a correct match is the *selection of surface features* (Sec. 1.3.2).

In the *descriptor representation* stage, global or local surface information is extracted, which can be used for surface comparison purposes during the optimization stage. This information is called a *surface descriptor*. In order to make comparisons possible, a distance metric between two descriptor instances must be defined alongside the descriptor itself. The *error metric* is used to determine how two surfaces fit to each other in any given stage of the matching process. *Optimization* denotes the process of finding a match between the input surfaces, such that the error metric is minimized. After the establishment of correspondences, a mapping between the input surfaces is computed on the *transformation* stage. Note, however, that the computation of a transformation does not necessarily occur only after the optimization stage is finished. In several methods, transformations are computed during the optimization process in order to identify correspondence sets with minimal error.

Generally speaking, given two surfaces represented by point samples, a source surface $S = \{si\}$ and a target surface $T = \{tj\}$, where si and tj denote the surface samples for source and target surfaces, respectively, their descriptors DS and DT, and an error metric $E(\cdot)$, the goal of surface matching is to find a mapping $\Phi : S \rightarrow T$ represented by a transformation operator $A : S \rightarrow T$, so that:

$$\Phi = \arg\min_{A} E(S, T, DS, DT, A) \qquad (1)$$

0.3.1 Descriptor Representation

Descriptors are pieces of information extracted from surfaces in order to make the comparison between two surfaces, or two surface parts, possible. They can be local or global, and can be used to subdivide the surfaces into regions with similar properties. Descriptors must be comparable to each other and, along with the descriptor itself, a distance metric between two descriptor entities has to be defined as well. For intra-operative registration purposes, the descriptor must be able to provide robust characterization even in the presence of noise. Another aspect to be considered is the discriminative power of the descriptor: If the descriptor is too sensitive, a small variation on the surfaces will result in a high distance value between the descriptors. As surface-based intra-operative registration must deal with surfaces acquired from different sensors and, therefore, different acquisition principles, variations on the surface representations for the same anatomical location should be expected. In this case, an over-sensitive descriptor would be inadequate. However, as scanned surfaces are usually nearly flat, since they have only a partial view of the object-of-interest, a certain degree of sensitivity is required in order to effectively discriminate the different regions of the surface. Since obtaining a perfect balance in discriminative power is very difficult, the optimization procedure must be able to deal with this issue. Furthermore, as we deal with partial surfaces, the descriptors should be able to represent information in local scales, instead of global ones. In addition, the descriptor should be invariant with respect to the occurring transformation class (see Sec. 1.3.5).

The most basic form of a surface descriptor is the surface *geometry* itself, *i.e.*, its points, edges, and faces. Geometry was used to find the set of four congruent points that, when mapped to each other, delivers an alignment with the maximal intersection area [95]. This method is robust to noise and very effective for rigid registration. Geometry was also used to search for a mapping between two surfaces, which minimizes some kind of deformation error between them [96, 97]. Although these approaches are very effective, they are time-consuming and usually not applicable for surfaces without prominent features (see Sec. 1.3.4). Another class of methods that employs geometry as a descriptor are the variants of the *iterative closest point* algorithm (ICP) [98], which iteratively finds pairs of closest points and computes a transformation that maps these points onto each other (see Sec. 0.3.4.2 for more details). This class of methods is employed for the fine alignment of surfaces as well as for accounting for displacements that occur in local scales, as an initial alignment must be provided in order to ensure convergence to the global minimum distance. Other methods for the fine alignment of surfaces based on pure geometric information were presented by Eckstein et al. [99], Papazov and Burschka [100].

Based on geometry, a global form of shape description is the *principal component analysis* (PCA) [101], which computes the principal axes of shape variation, using the eigenvectors associated with the largest eigenvalues of the second order moments covariance matrix. Matching two shapes using PCA implies aligning their principal axes. As mentioned before, PCA can usually only be used for aligning entire surfaces, as the principal axes extracted from a partial surface are incompatible to the ones extracted from the whole surface. Furthermore, PCA does not provide directions of the principal axes, thus matching solely based on PCA can be ambiguous.

Bronstein et al. [102], Eckstein et al. [99], Papazov and Burschka [100], Sahillioğlu and Yemez [103] employed *geodesic distances* for matching. A geodesic is defined as a curve which realizes the shortest distance between any two points lying on a general metric space [104]. In the case of surfaces (2-dimensional embeddings), the geodesic distance between two points lying on a surface denotes the length of the shortest line above the surface that connects these two points (Fig. 4). Only relying on geodesic distances for matching, can be inconclusive in the intra-operative case, as surfaces are mostly nearly planar, and every point has similar geodesic fields (Fig. 4b), differently from surfaces that have a more complex structure (Fig. 4c). Furthermore, geodesic distances are not robust to noise. Distances are usually longer on noisy surfaces because of the high frequency variations on the surface. A slightly improved form of point (local) descriptors, which considers the discrete approach of geometry of its neighbors but not the global geometry, are the principal curvatures and other curvature-based quantities (Fig. 5): *Mean curvature*, *Gaussian curvature* [105], *shape-index*, and *curvedness* [106].

Figura 4: Geodesic distance fields for two distinct points on different surfaces (red: high, blue: low): (a) A plane. Both points have exactly the same radial geodesic field. (b) A porcine liver surface acquired by a time-of-flight camera. As the surfaces are nearly planar, the geodesic fields of both points are similar. They are also very similar to the radial fields on the plane surface. (c) A humanoid shape. As the structure is more complex than the previous surfaces, not resembling a plane, distinct points on the surface have different geodesic fields (unless they lie close to each other)

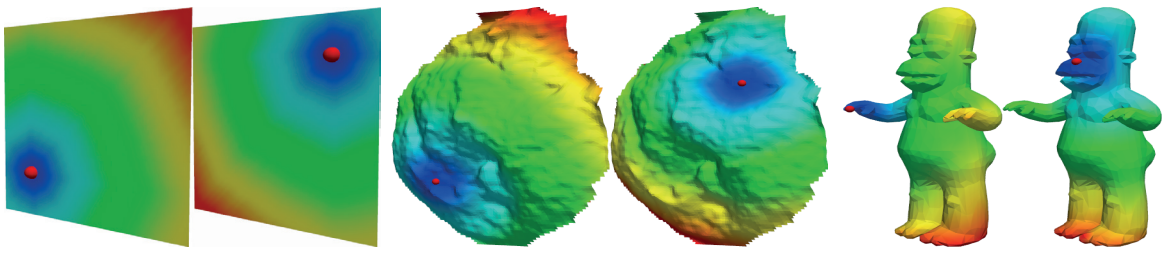

(a) (b) (c)

Figura 5: Mean curvature plot on a porcine liver surface acquired by a time-of-flight (ToF) camera. (a) Curvature computed according to Meyer et al. [105] on the original surface (noisy); (b) Curvature computed according to the same approach on the smoothed surface; (c) Curvature computed according to the noise-robust approach of Cazals and Pouget [107] on the original surface. The curvature values on the smoothed surface (b) and on the original surface computed with a more robust approach (c) are highly similar

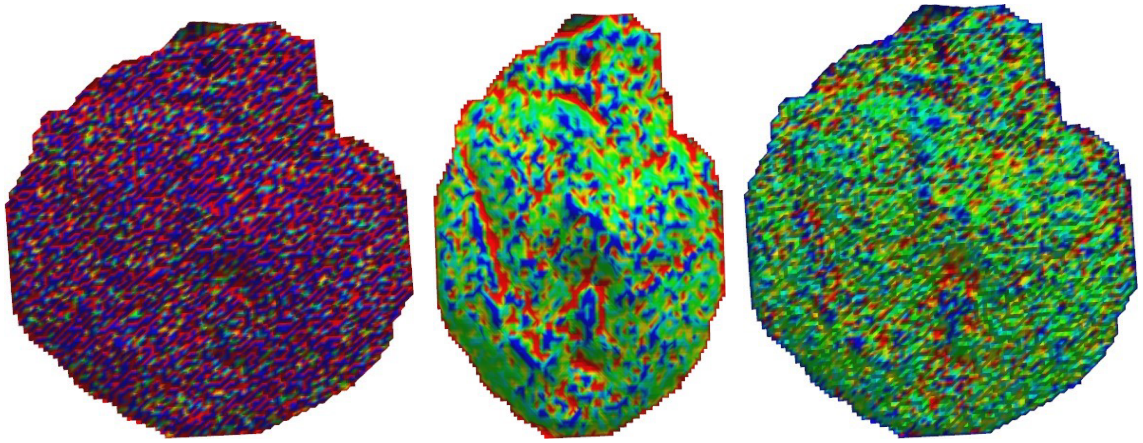

These measures are related to the way a surface bends in a particular point, *i.e.*, how the surface differs from a plane at a particular point. As the computation of curvatures on discrete surfaces is not robust to noise, Cazals and Pouget [107] proposed a method for the computation of differential properties by fitting a smooth polynomial to the local neighborhood, followed by computing the curvatures of this polynomial (Fig. 5c). Curvatures have been used as descriptors for many years. Kehtarnavaz and Mohan [108] segmented the surfaces in patches of homogeneous curvature and employed graph matching to obtain correspondences between them. Other methods employing curvature as a measure for data likelihood were presented by Zeng et al. [97, 109], Windheuser et al. [110]. The problem, however, is that there may be many points on one surface that have the same curvature values as another point on the other surface [111]. Curvatures are also used to select features on the surface, in order to reduce the search-space for correspondence search and to increase the chance of finding correct matches by using only more prominent and distinguishable points (see Sec. 1.3.2).

In order to increase the discriminative power and robustness of the curvature descriptor, Gatzke et al. [112] subdivided the geodesic circle around a particular point in bins, and computed the average curvature for each bin. The descriptor itself is represented by a vector, where a curvature average is stored at each vector's position, and each position represents the curvature value of a particular bin. Two descriptor entities are compared by means of the $L2$ norm. Johnson and Hebert [113, 114] presented the *spin-images* (Fig. 6), one of the most well-known descriptor for shape matching. Using the same idea of binning, they computed a 2D histogram of points that are contained inside a spherical volume by means of a plane rotating around the normal of a particular point.

Figura 6: Spin images for three points on the surface of a duck model (image found in [114])

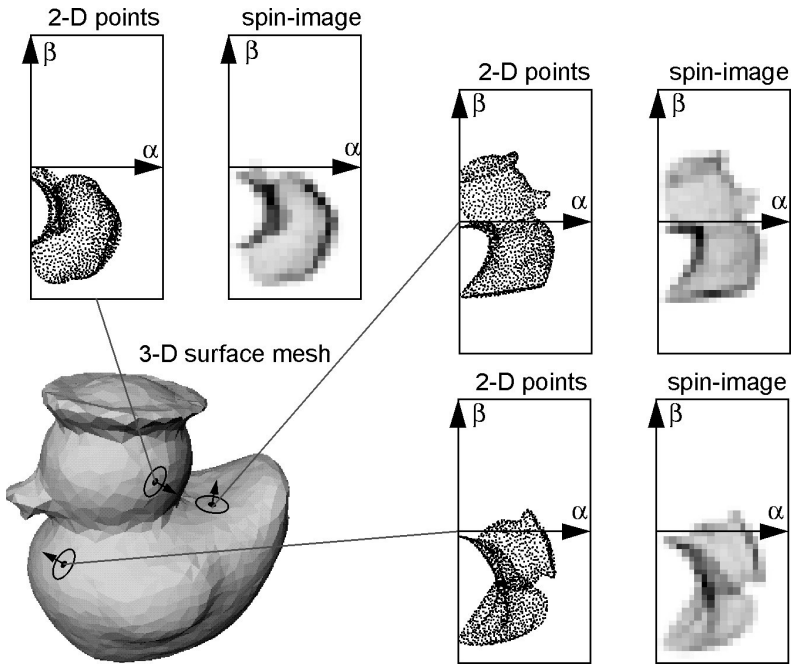

The descriptor proposed by Frome et al. [115], known as *3D shape context*, extends the idea of spin-images for a 3D spherical volume defined around a point, thus partitioning the sphere in bins by inserting subdivisions in the radial, azimuth, and elevation directions. However, in order to consistently index the 3D bins to the 2D vector that represents the descriptor, they rely on the determination of a local coordinate system for each point, which must be repeatable across surfaces. The same applies to the fingerprint-like descriptor presented by Sun and Abidi [116], Sun et al. [117], which is obtained by the projection of geodesic circles around a point to its tangent plane. Tombari et al. [118, 119], dos Santos et al. [120] improved the robustness of the computation of local coordinate systems, and presented the *signature of histograms* descriptor, which computes histograms of angles between normals, instead of computing histograms of point positions. The *MeshHog* descriptor [121] also applies an improved computation procedure of the local coordinate system, and computes histograms of mean curvature gradients. The robustness and repeatability of several descriptors based on the computation of local coordinate systems was investigated by Petrelli and Di Stefano [122], who performed several experiments with meshes of different point densities and noise levels.

For the global description of closed, articulated surfaces, skeletonization methods have been employed (Fig 7) [123, 124, 125, 126]. Skeletons naturally incorporate the notion and the representation of parts and articulations.

Figura 7: Matching a dog to different four-legged animals with different surface details by means of comparison of their surface skeletons (image found in [130])

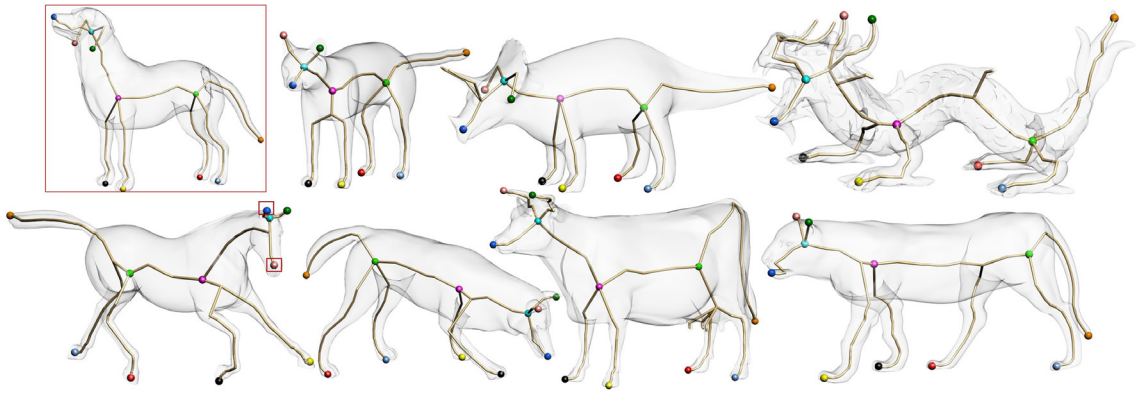

They are represented by trees, and matched by minimizing the differences between properties of branches and nodes. Global shape representations were also presented by Toldo et al. [127], Bronstein et al. [128], who computed a geometric vocabulary by clustering the descriptor space, which could be any local descriptor in this case. Each point descriptor is then represented in the vocabulary using vector quantization. The global descriptor is computed as the histogram of quantized local descriptors.

Gelfand et al. [111] computed the volume of the intersection between a sphere centered on a point and the surface for local shape description. This descriptor is called *integral volume descriptor*. Pottmann et al. [129] performed an analysis of robustness and stability of different integral computation methods, focusing on volume descriptors.

In a more elaborate manner of extracting surface information, authors represent surfaces as a series of functions of different frequencies (bands), defined on a sphere, in the same way as a Fourier series, but in 2D instead of 1D [131]. This technique is called *spherical harmonics*, and it can be employed for both the local and the global description of shapes. The global descriptors presented by Kazhdan et al. [132], Funkhouser et al. [133] store the amplitude of spherical harmonic coefficients within each frequency for shape retrieval in databases. Frome et al. [115], Funkhouser and Shilane [134] adapted this idea for local surface description, by constraining the spherical harmonics into local support volumes. Spherical harmonics have been extensively researched for the description of cortical surfaces (Fig. 8) [135, 136, 137]. An advantage of this representation is its robustness to noise when using lower frequency bands only, as noise is generally represented by higher frequencies.

More recently, attention has been drawn to the *manifold harmonics* [138, 139, 140, 141, 142], which are a generalization of the spherical harmonics for arbitrary manifolds. Importantly, the spherical harmonics are related to the manifold harmonics: the manifold harmonics series on a sphere is exactly the basis of the spherical harmonics series [139].

The advantage of the manifold harmonics representation is that it is invariant to isometric deformations[3], even

Figura 8: Representation of the cortical surface by spherical harmonic series of different highest frequency bands (image found in [135]). From left to right, the highest frequency band in the series decreases

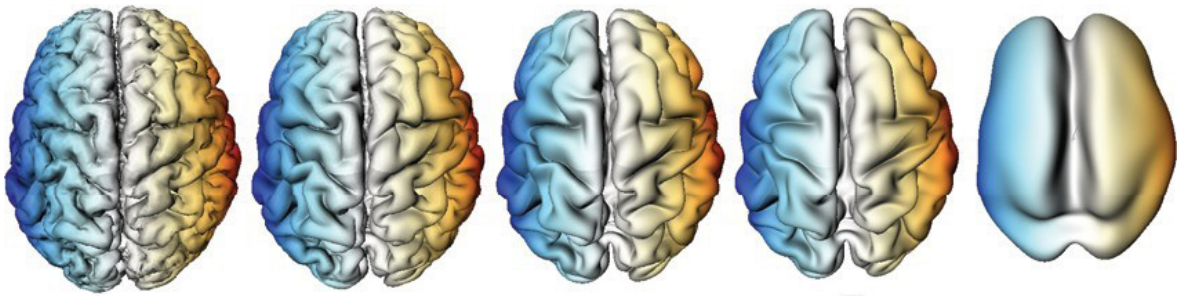

very large ones, as the frequency series is not defined on a sphere, like the spherical harmonics, but on the space spanned by the surface itself (Fig. 9a-b). Reuter et al. [145], Rustamov [146] employed manifold harmonic bands for noise-robust and isometry-invariant registration and database retrieval of complete models. However, because manifold harmonics are defined in the surface space, instead of a common space, it is not applicable to the registration of partial surfaces, since the manifold harmonic bands are incompatible and only make sense in the surface space itself (Fig. 9c). Furthermore, their computation is very expensive, as it involves the computation of eigenvalues and eigenvectors of large Laplacian matrices.

Based on the manifold harmonics, Sun et al. [147] presented the *heatkernel signatures* (HKS), which model the amount of heat that is transferred between two points in a given amount of time, assuming one of the points as a heat source.

As this descriptor is defined between two particular points, similar to the geodesic distance, and not on a global scale, like the manifold harmonics, it can be used for the registration of partial models. Dey et al. [148], Zobel et al. [149] improved the HKS for better registration and retrieval of partial and incomplete models. Although the computation of heat diffusion is noise robust, in contrast to geodesic distances, the diffusion in time occurs inversely proportional to the geodesic distance (Fig. 10). This implies higher amount of heat transfers occurring in shorter distances in shorter time. Thus points on nearly planar or planar surfaces have approximately the same heat diffusion fields, as they have similar geodesic distance fields. For the same reasons as mentioned for the geodesic distance fields, heat-based descriptors can be ambiguous for matching surfaces of

[3]Quoting from Beardon [143, p. 89]: A map f : R3 → R3 is an isometry if it preserves distances; that is, if for all x and y, ||f (x) − f (y)|| = ||x − y||. Isometric deformations on surfaces means that distances are preserved in a geodesic sense. In the case of surfaces, being isometry-invariant means being invariant to initial shape alignment, translation, rotation, scaling, and non-rigid bending [144].

interest of intra-operative registration. In addition, as HKS is based on manifold harmonics, their computation is also very expensive.

Comparisons and surveys on descriptor representations were presented by Tangelder and Veltkamp [150], Bustos et al. [151], Iyer et al. [152], Bronstein et al. [153], Heider et al. [154].

0.3.2 Feature selection

Feature selection is the process of identifying surface points that are unique on the surfaces, *i.e.*, points that can be used as reliable landmarks for the matching process. For instance, such points can lie on the extremities of a surface (Fig.

Figura 9: Manifold harmonic bands of two Armadillo models, and one of the Armadillo's arm. The columns show the first, second and third bands of their manifold harmonics. As the models in rows (a) and (b) can be nearly mapped to each other by an isometry, the bands are similar, as the spaces spanned by these surfaces are similar. However, the partial surface in row (c) spans a different space, which is not isometric to the other models, thus inducing different bands, defined in its own space 11)

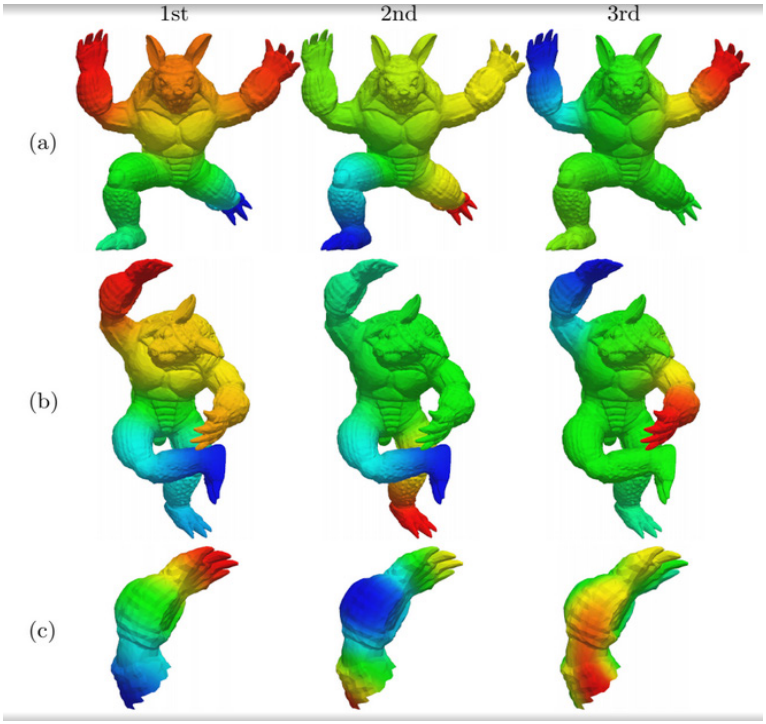

Figura 10: Figure 10: Heat diffusion field of a heat source (blue point) on different surfaces (red: high, blue: low), at different time points (125 and 500 seconds): (a) A plane. (b) A porcine liver surface acquired by a time-of-flight (ToF) camera. (c) A humanoid shape. The heat diffusion is inversely proportional to the geodesic distance (Fig. 4)

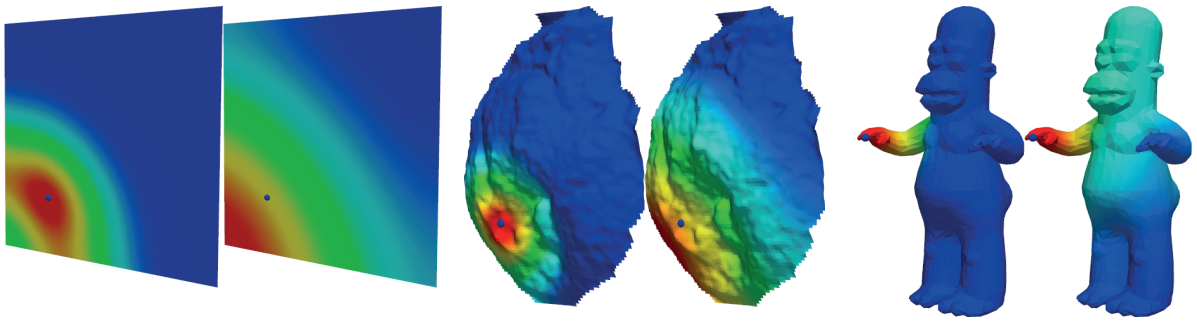

Feature selection is performed mainly for two purposes: First, to speed-up the registration by only using a subset of the data. Second, to increase the probability of finding a correct match between surfaces by using only prominent and reliable landmarks, and not the other more common points, which are more likely of having many similar ones. It is important to note, however, that, if feature selection is used, and correspondences shall be found only among the selected features, points lying on the same locations on both surfaces must be selected. If points lying on different locations are selected, finding a correct match between the surfaces is impossible. Consistent feature selection across surfaces is crucial for the successful registration of surfaces by methods relying on feature selection.

Methods for feature selection include: Random selection [155, 115]; Selection based on surface curvature [156, 157, 121]; Saliency [158, 159, 160]; Persistence across different scales [161, 111, 162, 163]; Number of similar points on the other surface [164]; Maximums of heat propagation [147, 165]; Tangential discontinuity [166]; Analysis of gradients [167, 168].

The consistent selection of features on surfaces of interest for intra-operative registration is not trivial. Because of the noise, lack of structure (no articulations), and lack of prominent and reliable landmarks (the surfaces are nearly flat), the consistent selection of features across pre- and intra-operative surfaces is usually not possible (Fig. 12). Methods for surface matching that rely on feature selection, are likely to fail in intra-operative registration scenarios.

0.3.3 Error metric

Error metrics are used to determine how well two surfaces match to each other in any given state of the optimization process. Error metrics can employ, among others, geometric information, descriptor similarities, or distortion measurements, in order to estimate an error value for the current optimization state. In Sec. 1.3.3.1 we focus on error metrics that are used to establish correspondences between points, while in Sec. 1.3.3.2 we show some error metrics for establishing correspondences between other kinds of non-point-based descriptors, such as regions and skeletons.

Figura 11: Features selected from two different dog surfaces (image found in [96]). Note that features are consistently selected on both surfaces, *i.e.*, they are chosen on the same locations

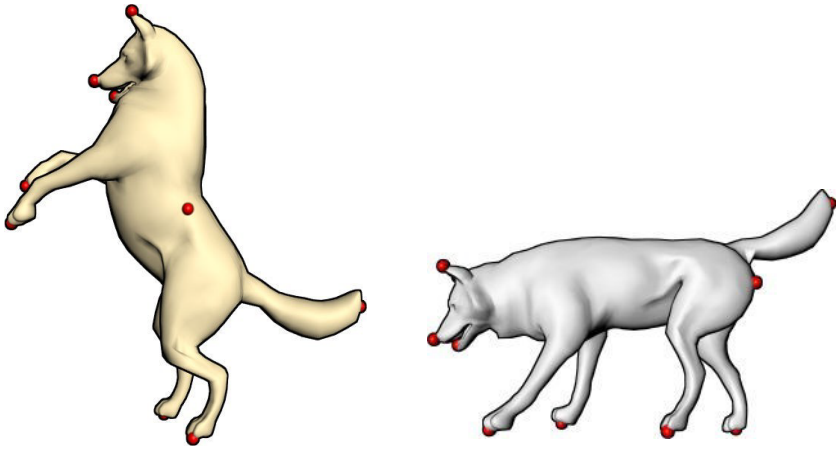

Figura 12: Comparison between selected feature points on two surfaces of the same object (porcine liver), as acquired by a computed tomography (left) and a time-of-flight (ToF) camera (right). Features were selected according to the multi-scale approach of Ho and Gibbins [163]

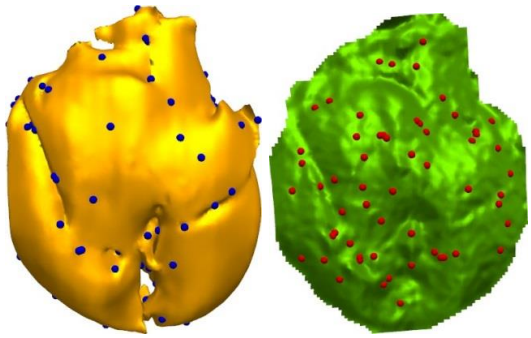

0.3.3.1 Error metrics for point correspondences

Let us assume two surfaces represented by discrete samples (points): The source surface $S = \{s_i\}$, and the target surface $T = \{t_j\}$. The goal is to find a set of correspondences $C \subset S \times T$ between source and target surfaces that delivers the best alignment with respect to an error metric when these correspondences are used to compute a transformation that aligns both surfaces. The set C is defined by its characteristic function $\sigma C: S \rightarrow T$, which is partial and injective, *i.e.*, not all points have correspondences, but the ones that do have a correspondence, have a single one.

The most basic form of error metric is the Euclidean distance $d\text{Eucl}(\cdot,\cdot)$ between source and target points. Using the closest point for finding correspondences, the correspondence set can be obtained as follows:

$$C = \{(Si_2\ tj): tj = \arg\min_{tk \in T} d_{Eucl}(Si_2\ tk)^2\}$$

If the surfaces are aligned closely enough, the closest point is a simple way of finding correspondences. In practice, however, it is very unlikely to find cases where the closest point could deliver a correct correspondence set. Nevertheless, there exists an entire class of iterative algorithms, derived from the *iterative closest point* (ICP) algorithm [98] (see Sec. 1.3.4.2), that minimizes the global squared Euclidean distance:

$$E_{ICP}(S,T) = \sum_{Si \in S} d_{Eucl}(S_i, \arg\min_{tj \in T} d_{Eucl}(si, tj))^2$$

Note that the error metrics presented so far do not incorporate any kind of similarity between points, relying only on geometric information[4].

Let us assume the function $q: S \times T \rightarrow R$ that measures the incompatibility between a point on the source surface and one on the target surface, based on their descriptor distances, for example. A simple error metric that incorporates these incompatibility values is defined as the *linear assignment problems* (LAP) [169], which computes the global compatibility error of a correspondence set:

$$E_{LAP}(C) = \sum_{(Si2tj) \in EC} q(Si,tj)$$

[4]Note that there are variants of the ICP algorithms that do incorporate other kind of similarity metrics. See Sec. 0.3.4.2 for more references on this topic.

The optimization of ELAP(·) delivers the correspondence set with minimal global incompatibility. In contrast to EICP(·,·), ELAP(·) does not incorporate any kind of geometric information, solely relying on incompatibility measurements between points. A more sophisticated error metric is defined as the *quadratic assignment problem* (QAP) [169], which not only incorporates a first order incompatibility measure such as $q(\cdot)$, but also includes a second order regularization (smoothing) term, which measures the incompatibility between assignments:

$$EQAP(C) = \sum_{(S_j,t_j)EC} \sum_{(S_k,t_j)EC} q2(S_i,S_k,t_j.t_l) + \sum_{(S_j,t_j)EC} q(S_i,t_j)$$

where $q_2 : S \times S \times T \times T \rightarrow R$. Incompatibility between assignments can be measured, for example, as the difference between the distances of source points

Figura 13: Registration of several partial surfaces of a bunny using the EdRMS(·) (see Eq. 6) error metric (bottom left) and after the error minimization of the initial registration with ICP (bottom right)

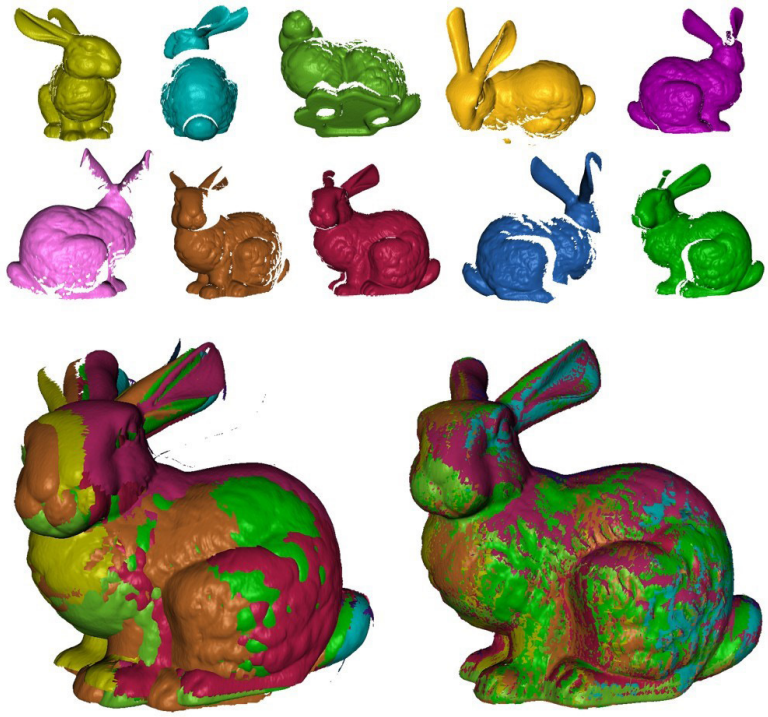

and their corresponding ones ($d_{Eucl}(s_i, s_k) - d_{Eucl}(t_j , t_l)$). This means if s_i is assigned to t_j and s_k to t_l, we expect the Euclidean distance between s_i and s_k to be equal to the distance between t_j and t_l, in a rigid case. Employing EQAP(·) for registration problems is a more robust compared to ELAP(·), as, like ELAP(·), it is independent of the initial position of the surfaces, but permits the incorporation of both geometric and descriptor similarities. Unfortunately, Sahni and Gonzalez [170] showed that QAP is NP-hard, and even finding a nearly optimal solution, within some constant factor, cannot be performed in polynomial time.

Gelfand et al. [111] showed that a pure second order, Euclidean distance based error is robust enough to rigidly match partially overlapping surfaces (Fig. 13). They employed the *distance root mean squared* (dRMS) error, which is similar to the second order definition presented above,

comparing all internal pairwise distances between corresponding points:

$$\underset{=}{E}\,\mathrm{dRMS}(C) \frac{1}{|C|^2} \Sigma\ \Sigma\ (d_{Eucl}(S_i,S_k) - d_{Eucl}(t_j,t_l))^2$$

The solution of the registration problem using this metric is a QAP and, therefore, NP-hard (see Sec. 1.3.4 for a discussion on the optimization procedures). Funkhouser and Shilane [134] employed a full QAP error metric for rigid registration, incorporating not only the second order term based on distances, but also the first order term, based on point dissimilarity measures. Chang and Zwicker [171] applied the same QAP error metric, but for the problem of matching shapes undergoing isometric deformations. They identified surface patches that were subjected to the same rigid transformation, and solved the registration as a labeling problem.

For the registration of shapes undergoing isometric deformations, the adaptation of the QAP error metric can be performed in a straightforward manner, by replacing the Euclidean distance with the geodesic distance (Fig. 14).

Figura 14: Correspondences obtained for a pair of hand model using the Eiso(·) (see Eq. 7) error metric for registration under isometric deformations (image found in [172])

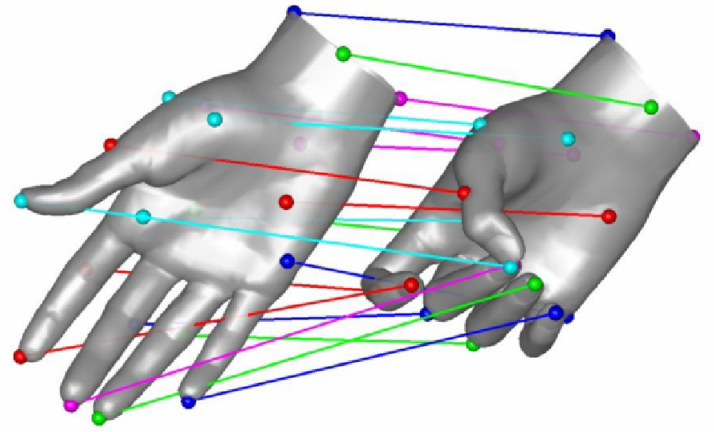

Sahillioğlu and Yemez [103] employed only the second order term, directly replacing the Euclidean distances in the *E*dRMS(·) formulation with the geodesic distance, while Dubrovina and Kimmel [172], Wang et al. [173] formulated their error metrics as a full QAP error, as follows:

$$E_{iso}(C) = w \sum_{(Si,tj)EC} \sum_{(Sk,tj)EC} (d_{geo}(si,sk) - d_{geo}(t_j,t_l)) + \sum_{(si,ti)EC} q(s_i,t_j)$$

where $d_{geo}(\cdot,\cdot)$ denotes the geodesic distance between two points on the same surface, $q : S \times T \rightarrow R$ a function that measures the incompatibility between a point on the source surface and one on the target surface, and w a weighting scalar to balance the influence of the terms. Raviv et al. [174] used the same error metric formulation, but instead of using geodesic distances, they employed heat diffusion as a distance metric. As explained in Sec. 1.3.1, heat diffusion is inversely proportional to the geodesic distance, with the advantage of being robust to noise.

Lipman and Funkhouser [175], Zeng et al. [97, 109] employed the deformation error between source and target surfaces,

when they are both conformally flattened onto a common canonical 2D domain, as their error metric. This flattening can be uniquely determined by fixing any three points on the surface. Zeng et al. [97, 109] posed this flattening error as a third order assignment problem, as follows:

$$E_{2D\,fit}(C) = \sum_{(s_j,t_j)EC} \sum_{(s_k,t_j)EC} \sum_{(s_m,t_n)EC} \theta(s_i,s_k,s_m,t_j,t_l,t_n) + q(s_i,t_j)_{(s_j,t_j)EC}$$

where $\theta : S \times S \times S \times T \times T \times T \rightarrow \mathrm{R}$ denotes the mutual flattening deformation error.

Dos Santos et al. [176] introduced a measure of point configuration error, which can be used to weight the fitting error in cases where no reliable feature detection is possible. Zhang et al. [96] utilized an error metric that measures elastic distortion and preservation of local differential properties for an as-rigid-as-possible deformable mapping [177, 178] of the entire surface S onto surface T , given a set of k correspondences. Windheuser et al. [110] employed an error metric defined by the elasticity theory as commonly known in physics, which measures stretch and bending error [179,180]. They posed the error as a linear error metric, computing it for pairs of triangles.

0.3.3.2 Other error metrics

The measurement of errors not related to point correspondences and relations between point correspondences can also be found in the literature. However, they are not as commonly used as the ones presented in the previous section (Sec. 1.3.3.1). As in the previous section, we assume two discretely sampled surfaces $S = \{si\}$ and $T = \{tj\}$, the source and target surfaces, respectively.

The most common metric for measuring the global error between two surfaces is the *Hausdorff distance* [181], which is based on the Euclidean distance. This metric computes the maximum of the distances from a point in any of the surfaces to the nearest point on the other surface. In its discrete form, the Hausdorff distance is defined as follows:

$$E_{\mathrm{Hausd}}(S,T) = \max\{\max_{s_i \in S} \min_{t_j \in T} d_{\mathrm{Eucl}}(s_i,t_j), \max_{t_j \in T} \min_{s_i \in S} d_{\mathrm{Eucl}}(s_i,t_j)\} \quad (9)$$

Note that the Hausdorff distance is symmetric, *i.e.*, $E\mathrm{Hausd}(S, T) = E\mathrm{Hausd}(T, S)$. Charpiat et al. [182], Eckstein et al. [99] proposed the *pseudo-Hausdorff distance*, which has the advantage of being differentiable with respect to the position of the points of the two meshes [99]. The pseudo-Hausdorff distance converges to the Hausdorff distance with increasing sampling of the surfaces [182]. A global distance metric for isometrically deformed surfaces is the *Gromov–Hausdorff distance* [183], which measures how far two surfaces are from being isometric. The Gromov-Hausdorff distance, in its discrete form, is defined as follows:

$$E_{\mathrm{Gro\text{-}Hausd}}(S,T) = \inf_{f,g} E_{\mathrm{Hausd}}(f(S), g(T)) \quad (10)$$

where $f : S \rightarrow Z$ and $g : T \rightarrow Z$ are isometric embeddings into the metric space Z. Note the similarity with the error metric presented by Lipman and Funkhouser [175], Zeng et al. [97, 109] (see Sec. 1.3.3.1, Eq. 8), where they measure the deformation error of the embeddings of both surfaces onto a 2D plane.

Aiger et al. [95] used the size of the intersection region between two surfaces as a similarity metric, measured as the amount of points on one surface that are close enough (smaller than a given threshold) to a point on the other. Au et al. [130] adopted the amount of votes casted by all reasonably possible combinations of fitting two skeletons to each other as similarity values for skeleton nodes.

0.3.4 Optimization

Two classes of optimization methods are known in surface matching: The first aims to find a set of correspondences that roughly aligns two shapes and is called *rough-scale optimization* (Sec. 1.3.4.1). This kind of optimization is usually automatic, *i.e.*, it makes no assumptions about the initial position of the surfaces in space. Most rough-scale optimization methods deliver a sparse set of correspondences. The second class of optimization contains the methods that account for small misalignment and for deformations in the local scale. This class of optimization is therefore called *fine-scale optimization* (Sec. 1.3.4.2). It contains the popular *point-based iterative optimization* algorithms, such as the *iterative closest point* (ICP) [98] and its variants.

An extended bibliography on correspondences search for surface matching problems was presented by van Kaick et al. [184].

0.3.4.1 Rough-scale optimization

One of the simplest solution for obtaining an automatic matching between two surfaces is to minimize the *linear assignment problem* (LAP) error using the distance between descriptors (see Sec. 1.3.1) as a measure of dissimilarity between points. Minimizing the LAP error metric is equivalent to obtaining a set of point correspondences between source and target surfaces, so that every point on the source surface is assigned to its most similar point on the target surface, in a way that the sum of the distances between the descriptors of assigned points becomes the minimum. As can be seen in Eq. 4, the error metric minimized for the solution of the LAP does not contain any information about the relative position of the surfaces, which is irrelevant for this problem. The LAP is one of the oldest and most studied problems in combinatorial optimization [185] and there are several algorithms to solve it in polynomial time. Under certain conditions, it can even be solved in linear time (see [185] for a review on these algorithms).

However, solving the surface matching problem as a LAP may be error-prone for two reasons: (1) As LAP only considers descriptor similarities, and usually there are multiple correspondence configurations with compatible descriptors, finding the correct match may be difficult, as the problem becomes very ambiguous; (2) As LAP does not incorporate any regularization term, ensuring that points in a particular neighborhood on the source surface will be assigned to points that also belong to a common neighborhood on the target surface, it may result in a lack of geometric consistency among correspondences. Furthermore, it is important to note that the formulation

of the surface matching problem as a LAP finds a global matching between the possible correspondences. This means that a correspondence will be assigned for every point on the source surface, assuming that the source surface has less points than the target one, and that no feature selection was performed. If the surfaces represent areas that are only partially overlapping, solving a global assignment problem cannot, in any manner, deliver a correct set of correspondences, as the points that do not belong to the overlapping area should be left unassigned. For partial surface matching, in the case of LAP, one can resort to the *k-cardinality assignment problem* (CAD) [186]: Given an integer k, one wants to find k correspondences from source to target surface, so that the sum of distances between the descriptors of corresponding points becomes the minimum.

The *quadratic assignment problem* (QAP) error (Eq. 5 on page 19) incorporates a regularization term for neighborhood consistency of the correspondences. However, solving a QAP is known to be NP-hard [170]. Still, there are two common methods for solving QAP (see [187, 188] for more details): The first class of methods performs a combinatorial analysis based on search procedures, such as *greedy search* or *branch-and-bound* [189]. Although a full combinatorial analysis of the correspondences space guarantees that the global minimum is found, it may be untreatable to search the entire space. Therefore, many authors resort to measures that constrain and reduce the search-space. The second class of methods is known as *probabilistic relaxation* [190], where the constraints of the QAP are relaxed to allow fuzzy correspondences, casting the problem as a convex continuous minimization problem. Although the problem becomes treatable due to relaxation, it is prone to follow into a local minimum. In the rest of this section, we review the solutions found in recent publications on surface matching.

Branch-and-bound optimization was employed by Gelfand et al. [111], Dubrovina and Kimmel [172], Raviv et al. [174]. While Gelfand et al. [111] employed it for the minimization of the EdRMS$(\cdot)$ error metric (Eq. 6 on page 20), based on Euclidean distance, thus only applicable to rigid registration, Dubrovina and Kimmel [172], Raviv et al. [174] minimized the Eiso$(\cdot)$ error metric (Eq. 7 on page 21), which employs geodesic distance, thus being also applicable to the registration of isometrically deformed surfaces. Branch-and-bound is based on the enumeration of all possible solutions while discarding the solutions with an error greater than the current error. In fact, branch-and-bound optimization can be most efficiently implemented as a search-tree, where the correspondences are represented as nodes while a path from a leaf to the root determines a possible solution. During the construction of the search-tree, every time a new branch is added to a node, the error of this partial solution is computed: If the error rises above the current error, the branch is pruned, and the space is not searched in this direction anymore. Otherwise, the tree keeps expanding until the solution is complete. The path with the smallest error is the correspondence set with minimum error. In order to reduce the search-space, the authors employ feature selection, feature clustering, distance

consistency tests during tree construction [111].

Funkhouser and Shilane [134], Zhang et al. [96], Au et al. [123], Sahillioğlu and Yemez [103] used a *constrained greedy optimization* approach, or *exhaustive search*, which enumerates and tests the entire search-space. For faster computing, they employed several constraints to reduce the search-space before starting the optimization. Importantly, a common search-space constraining measure was adopted by all of them: the selection of very few and trustworthy features. Funkhouser and Shilane [134] performed a priority-driven search, which biases the correspondence search towards correspondences between features with smaller descriptor distances. As their method focuses on rigid registration, descriptor distances are a highly reliable measure, as descriptors at the same locations on two different rigid structures are very close to each other. Zhang et al. [96] presented a powerful method for matching non-isometric surfaces, where the set of correspondences that minimizes a deformation error is selected in a greedy optimization. However, the computation of the deformation error is very inefficient, as a large overdetermined linear system, representing the deformation for the entire surface, must be solved, in a least-squares sense. Au et al. [130] computes votes for plausible correspondences when aligning skeletons of different surfaces in all possible ways.

A common optimization technique in surface matching is known as *random sample consensus*, or *RANSAC* [191]. RANSAC follows the approach of iteratively selecting a given number of random samples from the correspondence search-space, computing a model (transformation) that maps these samples, and verifying how many other samples in the space also fit (consent) in the computed model. As random samples are selected in every iteration, the algorithm is non-deterministic, and produces a reasonable result only with a certain probability, which increases with increasing number of iterations. RANSAC is also known as a *voting technique*, as other samples "vote" for a given model. Aiger et al. [95] select random sets of four congruent points, aligns them rigidly, and counts the number of points that are also aligned, *i.e.*, whose distance is smaller than a given threshold. Tevs et al. [192] employed a RANSAC loop for minimizing a QAP error, but biased the randomly sampling towards sample sets with higher probability of being correct correspondences. Lipman and Funkhouser [175] projected isometric surfaces onto a 2D canonical domain, and aligned them rigidly in this domain by computing a transformation between three point correspondences selected in a RANSAC-loop, and then casted votes for further correspondences based on the distance of closely aligned points.

Projecting the surfaces onto a canonical domain, where distances can be measured as Euclidean distances instead of geodesic distances, allows the matching between them to be performed rigidly. In this case, the alignment can be performed by any robust and efficient method for rigid registration (*e.g.* [111, 95]). It also profits from a distance metric that can be efficiently computed - the Euclidean distance - and from reliable descriptor distances. In surface matching, popular

techniques for embedding surfaces in common spaces are the *multidimensional scaling* (MDS) [193], which embeds the surfaces in a common R*n* space, and the *generalized MDS* [102], which embeds one surface into the space spanned by the other, thus eliminating distortions that may arise from a R*n* embedding. Unfortunately, these methods share a drawback: They require the repeated computation of geodesic distances for obtaining the embedding, which is not efficient. In the work of Lipman and Funkhouser [175], a more efficient technique for flattening was employed, based on the works of Pinkall et al. [194], Polthier [195].

Another common technique for solving QAPs is *relaxation*. In this approach, the binary constraints are relaxed to a fuzzy domain, posing the problem as a convex optimization problem. In surface matching, the relaxed QAP problems are usually cast as a *graph labeling problem*, where a label (correspondence) is searched for each point on the source surface (see [196] for more details on graph labeling). Popular algorithms for solving the graph labeling problem are the *maximum-flow/minimum-cut* algorithms [197,198,199], which poses the search-space as a system of pipes, with widths given by similarity values. These algorithms search for sub-systems with maximum flow for determining correct labeling. Zeng et al. [97], Wang et al. [173] solved the surface matching problem as a graph labeling problem. Zeng et al. [97] employed a third order error metric (Eq. 8 on page 21) for computing a deformation error based on flattening, as presented by Lipman and Funkhouser [175]. In order to formulate the problem as a QAP, they considered the observation that any relaxed high-order term can be reduced to quadratic terms [200, 201] and solved it as a set of QAPs. Zeng et al. [109] presented a more efficient method for solving the high order error terms, using a *Markov random field* optimization algorithm [202], thus casting the problem as a linear program. Relaxation can also be used to minimize LAPs [203], and has been employed in surface matching by Windheuser et al. [110]. Here, the authors minimize a linear error metric based on stretching and bending energy. The solution of surface matching problems by means of relaxation and labeling algorithms is usually very computationally expensive, and the selection of very few features is therefore mostly a requirement. dos Santos et al. [204] approximated the solution of a QAP by firstly iteratively computing similarity scores between surface neighborhoods, generating a similarity matrix, and then computing assignments by directly solving a LAP.

Note that, similar to LAP, the direct minimization of the QAP error is global, and does not account for partially overlapping data. If the overlapping region is sufficiently large, maximum-flow/minimum-cut algorithms for graph labeling solve this problem by incorporating a label for outliers.

0.3.4.2 Fine-scale optimization

Fine-scale optimization procedures are used for accounting for small misalignments and for deformations that occur in local scales. They usually assume that the surfaces have been roughly aligned or that an initial set of correspondences

is given. An important class of fine-scale optimization algorithms is the *point-based iterative optimization*, which contains the *iterative closest point* (ICP) algorithm [98] and its variants.

One of the most well-known classes for optimization of local scale deformations is known as *as-rigid-as-possible* (ARAP) [205, 206, 207, 208, 100], which deforms the source surface towards a set of few correspondences (anchors) by computing a fit that preserves, as much as possible, some surface properties (*e.g.* normal orientations [177, 178], or face Laplacians [209]). ARAP registration is usually obtained by minimizing a large overdetermined linear system of equations in a least-squares sense.

Given a coarse set of previously known correspondences, Tevs et al. [192], Wang et al. [173], Sahillioğlu and Yemez [103] iteratively solved local QAPs around the known correspondences, until a correspondence for every point was found, resulting in a dense set of correspondences. Zeng et al. [97] employed the same strategy (Fig. 15), but minimized instead a high-order error metric (Eq. 8 on page 21). Raviv et al. [174] incremented the initial sparse correspondences by a set of isometrically consistent correspondences, selecting the next correspondence candidates by a *farthest point sampling* strategy [210]. Sharma et al. [211] increments the initial correspondences set by pairs of points with consistent heat propagation, using an *expectation maximization* approach [212]. Eckstein et al. [99] fitted two roughly aligned surfaces by defining a differentiable global error metric between them (pseudo-Hausdorff distance, see Sec. 1.3.3.2), and solved the problem by a gradient descent approach.

Point-based iterative optimization

Point-based iterative optimization is the most well-known class for fine optimization. It is based on the *iterative closest point* (ICP) algorithm [98]. The ICP algorithm works as follows: (1) For each point on the source surface, the closest point on the target surface is found; (2) A rigid transformation that maps the pairs of closest points is computed; (3) The algorithm performs the two previous steps iteratively, until convergence is reached. It was shown that, in rigid settings, the ICP algorithm converges to at least a local minimum of the sum of squared Euclidean distances (Eq. 3 on page 19).

Figura 15: A set of initial sparse correspondences (a) and its expansion in a dense correspondence set (b) (image found in [97])

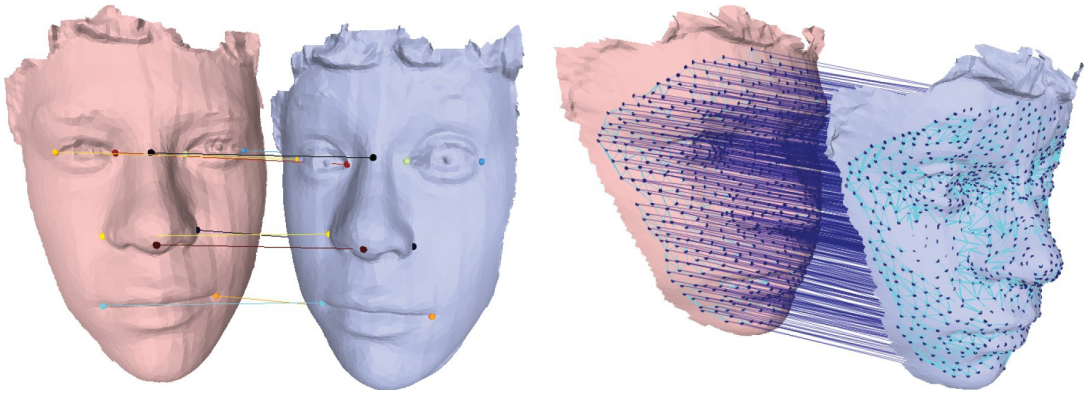

There are several variants of the ICP algorithm, dealing with: Better selection of correspondences [213,214,215]; Weighting of correspondences [216,213]; Robustness to the influence of outliers [217, 218]; Adequacy of the error metric [219, 220, 221]; Non-rigid deformations [222, 223, 224]; Anisotropic errors [225]. Focusing on intra-operative registration, Cash et al. [38] presented an ICP variant that identifies and aligns minimally deformed regions of the surfaces. A non-rigid deformation based on a *finite element model* formulation is subsequently computed. Clements et al. [39, 44] presented some efforts to increase the robustness of this ICP variant, by incorporating measures of saliency.

For more details on variants of the ICP algorithm, we kindly refer the reader to [216,226].

2.2.5 Transformation

In surface matching, authors usually consider three classes of transformation: *rigid*, *affine*, and *non-rigid*.

Rigid transformations are composed of rotations and translations. The shape of the object cannot be altered by means of rigid transformations. Given a set of correspondences, the computation of a rigid transformation that aligns these correspondences, such that the sum of their squared Euclidean distance is minimal, is usually performed by solving an overdetermined linear system, in a least-square sense [227].

Affine transformations are a generalization of the rigid transformations, removing some of the constraints of the rigid transform operator. Although not all affine transformations are angle preserving, lines remain parallel [228]. A specific affine transformation of interest for surface matching is scaling, where the dimensions of the object change, but angles are preserved. Given a set of correspondences, an affine transformation between them can be computed according to the method presented by Feldmar and Ayache [229], which also minimizes the sum of squared distances.

Non-rigid transformations, also known as *free-form* transformations, are subdivided in two classes: isometric and non-isometric. Isometric transformations preserve distances (geodesic distances),

while non-isometric do not. Non-rigid transformations are usually represented by *piecewise polynomials* [228], which model transformations for local surface patches while maintaining first or second order continuity between patches. This ensures a smooth mapping between the surfaces. Most well-known piecewise polynomials for transformations are the *thin-plate splines* [230] and the *B-splines* [231]. For more details on transformations, we kindly refer the reader to [228, 51].

1 CONCLUSIONS

In this paper, we presented a review of the most recent and influential techniques for surface matching, classifying them according to the descriptor, error metric and optimization method employed, and relating them to the problem of matching surfaces for intra-operative registration purposes. Tab. 1 provides an overview of these methods. Despite of the many advances in the field, we found that most of the rough-scale optimization methods for non-rigid surface matching rely on the solution of *quadratic assignment problems* (QAPs, see Sec. 1.3.3). In the context of surface matching for intra-operative registration, this implies two main drawbacks: First, QAPs uses the difference of distances between assigned point pairs as a regularization term. As shown in Sec. 1.3.1, these geodesic distance profiles are not sufficiently discriminative for nearly planar surfaces, such as the ones acquired in intra-operative environments, as they are for more complex shapes, such as a human form. Second, the direct solution of a QAP using a minimization technique, such as relaxation (Sec. 1.3.4.1), makes the registration of partially overlapping surfaces harder, as QAP would provide a global set of correspondences that minimizes the error.

Authors solved the first problem by the incorporation of higher order and more complex error metrics (*e.g.* [96, 97]). The second drawback was solved by an enumeration of the search space, for the desired amount of correspondences, and by solving the minimization problem with constrained greedy optimization procedures or voting schemes (*e.g.* [192, 103]). However, in these cases, the computational cost becomes so expensive that the consistent selection of features on both surfaces becomes a necessity, *i.e.*, a very few representative and unambiguous features that can be consistently selected from the same locations on both surfaces need to be selected. As discussed in Sec. 1.3.2, consistent feature selection on pre- and intra-operatively acquired surfaces is an issue, as these surfaces are nearly flat, and many distortions and deformations occur between them.

In conclusion, while suitable fine-scale optimization methods for intra-operative registration already exist [36, 37, 38, 39, 40, 41, 42, 43, 44, 45], the automatic alignment of surfaces of different modalities acquired pre- and intra-operatively by rough-scale optimization methods remains a challenge. Complete shape based registration approaches for

intra-operative purposes should be further investigated though, as they release the physician from the burden of placing and calibrating fiducial markers, and the patients from several radiological image acquisitions, usually exposing them to radiation. As nowadays most interaction and tracking solutions in entertainment systems are moving to surface-based approaches (*e.g.* Kinect®), so will be the future of the operating rooms.

Tabela 1: Overview of the state-of-the-art surface matching approaches. Refer to Secs. 0.3.1, 0.3.3, 0.3.4 and 0.3.5 for a description of the methods and of the abbreviations

Authors	Descriptor	Rough/fine scale	Optimization	Error metric	Global/ Partital matchin	Rigid/Non-rigid transformatio	Feature sele
Gelfand et al. [111]	Integral volume descriptor	Rough	Branch-and-bound	$E_{dRMS(-)}$	Partial	Rigid	Yes (on the source surface only)
Cash et al. [38]	-	Fine	Point-based iterative	Modified $E_{ICP(-)}$	Partial	Non-isometric	No
Funkhouser and Shilane [134]	Spherical harmonics	Rough	Greedy	QAP	Partial	Rigid	Yes
Eckstein et al. [99]	-	Fine	Gradient descent	Pseudo-Hausdorff distance	Partial	Isometric	No
Aiger et al. [95]	-	Rough	Voting	Size of intersection	Partial	Rigid	No
Zhang et al. [96]	Gatzke et al. [112]	Both	Greedy	ARAP deformation error	Partial	Non-isometric	Yes
Tevs et al. [192]	Histogram of mean Curvatures	Both	RANSAC	QAP	Partial	Isometric	Yes
Lipman and Funkhouser [175] dos Santos et al. [204]	-	Rough	Voting	Embedding deformation error QAP/LAP	Partial	Isometric	No
	Curvatures	Rough	Iterative similarty propagation		Partial	Isometric	No
Zeng et al. [97]	-	Both	Relaxation	$E_{2D\ fit(-)}$	Global	Non-isometric	Yes
Wang et al. [173]	HKS	Both	Relaxation	QAP	Global	Isometric	Yes
Au et al. [130]	Skeleton	Rough	Voting	Skeleton similarity	Global	Non-isometric	No
Dubrovina and Kimmel [172]	Manifold harmonics	Rough	Relaxation	QAP	Global	Isometric	Yes
Sahilliogu and Yemez [103]	-	Both	Greedy	QAP	Partial	Isometric	Yes
Windheuser et al [110]	-	Rough	Relaxation	Physics-based deformation error	Global	Isometric	Yes
Raviv et al. [174]	HKS	Both	Relaxation	QAP	Global	Isometric	Yes
Shama et al.	HKS	Fine	Expectation	QAP	Global	Isometric	No

REFERÊNCIAS

[1] N. Sugano, **Computer-assisted orthopedic surgery**, J. Orthop. Sci. 8 (2003) 442–448.

[2] R. Ewers, K. Schicho, G. Undt, F. Wanschitz, M. Truppe, R. Seemann, Wagner, **Basic research and 12 years of clinical experience in computer- assisted navigation technology**: A review., Int. J. Oral Max. Surg. 34 (2005) 1–8.

[3] T. M. Peters, **Image-guidance for surgical procedures**., Phys. Med. Biol. 51 (2006) R505–R540.

[4] Z. Yaniv, K. Cleary, **Image-Guided Procedures: A Review**, Technical Re- port, Georgetown University, 2006.

[5] S. DiMaio, T. Kapur, K. Cleary, S. Aylward, P. Kazanzides, K. Vosburgh, R. Ellis, J. Duncan, K. Farahani, H. Lemke, T. Peters, W. Lorensen, D. Gobbi, J. Haller, L. Clarke, S. Pizer, R. Taylor, R. Galloway, G. Fichtinger, N. Hata, K. Lawson, C. Tempany, F. Jolesz, **Challenges in image-guided therapy system design**, NeuroImage 37 (2007) 144–151.

[6] M. Baumhauer, M. Feuerstein, H.-P. Meinzer, J. Rassweiler, **Navigation in endoscopic soft tissue surgery: perspectives and limitations**., J. Endourol. 22 (2008) 751–766.

[7] B. J. Wood, J. Kruecker, N. Abi-Jaoudeh, J. K. Locklin, E. Levy, S. Xu, Solbiati, A. Kapoor, H. Amalou, A. M. Venkatesan, **Navigation systems for ablation**, J. Vasc. Interv. Radiol. 21 (2010) S257–S263.

[8] M. F. Khan, S. Dogan, A. Maataoui, S. Wesarg, J. Gurung, H. Ackermann, Schiemann, G. Wimmer-Greinecker, T. J. Vogl, **Navigation-based needle puncture of a cadaver using a hybrid tracking navigational system**., Invest. Radiol. 41 (2006) 713–720.

[9] J. Krücker, S. Xu, N. Glossop, A. Viswanathan, J. Borgert, H. Schulz, B. J. Wood, **Electromagnetic tracking for thermal ablation and biopsy guidance: Clinical evaluation of spatial accuracy**, J. Vasc. Interv. Radiol. 18 (2007) 1141–50.

[10] S. A. Nicolau, X. Pennec, L. Soler, N. Ayache, **Clinical evaluation of a respiratory gated guidance system for liver punctures**, in: Proc. MICCAI, 2007, pp. 77–85.

[11] E. B. Levy, J. Tang, D. Lindisch, N. Glossop, F. Banovac, K. Cleary, **Implementation of an electromagnetic tracking system for accurate intra-hepatic puncture needle guidance: Accuracy results in an in vitro model**, Acad. Radiol. 14 (2007) 344–354.

[12] E. B. Levy, H. Zhang, D. Lindisch, B. J. Wood, K. Cleary, **Electromagnetic tracking-guided percutaneous intrahepatic portosystemic shunt creation in a swine model**, J. Vasc. Interv. Radiol. 18 (2007) 303–307.

[13] J. Krücker, S. Xu, N. Glossop, W. F. Pritchard, J. Karanian, A. Chiesa, B. J. Wood, **Evaluation of motion compensation approaches for soft tissue navigation**, in: Proc. SPIE Med. Img.: Vis. Img.-Guided Proc. Mod., 2008.

[14] L. Maier-Hein, A. Tekbas, A. Seitel, F. Pianka, S. A. Müller, S. Satzl, S. Schawo, B. Radeleff, R. Tetzlaff, A. M. Franz, B. P. Müller-Stich, Wolf, H.-U. Kauczor, B. M. Schmied, H.-P. Meinzer, **In vivo accuracy assessment of a needle-based navigation system for CT-guided radiofrequency ablation of the liver**, Med. Phys. 35 (2008) 5385–5396.

[15] M. Baumhauer, T. Simpfendörfer, D. Müeller-Stich, D. Teber, C. Gutt, Rassweiler, H.-P. Meinzer, I. Wolf, **Soft tissue navigation for laparoscopic partial nephrectomy**, Int. J. CARS 3 (2008) 307–314.

[16] S. A. Nicolau, X. Pennec, L. Soler, X. Buy, A. Gangi, N. Ayache, J. Marescaux, **An augmented reality system for liver thermal ablation: design and evaluation on clinical cases**., MIA 13 (2009) 494–506.

[17] J. M. Fitzpatrick, J. B. West, C. R. Maurer, **Predicting error in rigid-body point-based registration**, IEEE TMI 17 (1998) 694–702.

[18] J. M. Fitzpatrick, J. B. West, **The distribution of target registration error in rigid-body point-based registration**, IEEE TMI 20 (2001) 917–927.

[19] A. Danilchenko, J. M. Fitzpatrick, **General approach to first-order error prediction in rigid point registration**, IEEE TMI 30 (2011) 679–693.

[20] S. Weber, M. Markert, T. Lüth, **Surface tracking of organs for registration in soft tissue surgery**, in: Proc. MICCAI IGSTI, 2008.

[21] M. Markert, A. Koschany, T. Lueth, **Tracking of the liver for navigation in open surgery**, Int. J. CARS 5 (2010) 229–235.

[22] L. Maier-Hein, A. Tekbas, A. M. Franz, R. Tetzlaff, S. A. Müller, F. Pi- anka, I. Wolf, H.-U. Kauczor, B. M. Schmied, H.-P. Meinzer, **On combining internal and external fiducials for liver motion compensation**, Comp. Aid. Surg. 13 (2008) 369–376.

[23] J.-S. Hong, T. Dohi, M. Hasizume, K. Konishi, N. Hata, **A motion adaptable needle placement instrument based on tumor specific ultrasonic image segmentation**, in: Proc. MICCAI, 2002, pp. 122–129.

[24] Z. Wei, L. Gardi, D. B. Downey, A. Fenster, **Oblique needle segmentation and tracking for 3D TRUS guided prostate brachytherapy**., Med. Phys. 32 (2005) 2928–2941.

[25] P. Bao, T. K. Sinha, C.-C. R. Chen, J. R. Warmath, R. L. Galloway, A. J. Herline, **A prototype ultrasound-guided laparoscopic radiofrequency ablation system**., Surg. Endosc. 21 (2007) 74–79.

[26] P. Hildebrand, M. Kleemann, U. J. Roblick, L. Mirow, C. Bürk, H.-P. Bruch, Technical **aspects and feasibility of laparoscopic ultrasound navigation in radiofrequency ablation of unresectable hepatic malignancies**., J. Laparoendosc. Adv. Surg. Tech. A. 17 (2007) 53–57.

[27] W. Wein, A. Khamene, D.-A. Clevert, O. Kutter, N. Navab, **Simulation and fully automatic multimodal registration of medical ultrasound**, in: Proc. MICCAI, 2007, pp. 136–143.

[28] M. Feuerstein, T. Mussack, S. M. Heining, N. Navab, **Intraoperative laparoscope augmentation for port placement and resection planning in minimally invasive liver resection**, IEEE TMI 27 (2008) 355–369.

[29] T. Lange, N. Papenberg, S. Heldmann, J. Modersitzki, B. Fischer, H. Lamecker, P. Schlag, **3d ultrasound-ct registration of the liver using combined landmark-intensity information**, Int. J. CARS 4 (2009) 79–88.

[30] J. Olesch, B. Beuthien, S. Heldmann, N. Papenberg, B. Fischer, **Fast intra-operative nonlinear registration of 3D-CT to tracked, selected 2D-ultrasound slices**, in: Proc. SPIE Med. Img.: Vis. Img.-guided Proc. Mod., 2011.

[31] L. Maier-Hein, Computer-assisted needle insertion - **Motion compensation and guidance**, Südwestdeutscher Verlag für Hochschulschriften AG Co. KG, 2009.

[32] A. Schweikard, G. Glosser, M. Bodduluri, M. J. Murphy, J. R. Adler, **Robotic motion compensation for respiratory movement during radiosurgery**, Comp. Aid. Surg. 5 (2000) 263–277.

[33] A. Khamene, J. K. Warzelhan, S. Vogt, D. Elgort, C. Chefd'Hotel, J. L. Duerk, J. S. Lewin, F. K. Wacker, F. Sauer, **Characterization of internal organ motion using skin marker positions**, in: Proc. MICCAI, 2004, pp. 526–533.

[34] C. Ozhasoglu, C. B. Saw, H. Chen, S. Burton, K. Komanduri, N. J. Yue, S. M. Huq, D. E. Heron, **Synchrony - Cyberknife respiratory compensation technology**, Med. Dosim. 33 (2008) 117–123.

[35] D. Sindram, I. H. McKillop, J. B. Martinie, D. A. Iannitti, Novel **3-D laparoscopic magnetic ultrasound image guidance for lesion targeting**, HPB 12 (2010) 709–716.

[36] A. Herline, J. Herring, J. Stefansic, W. Chapman, R. Galloway, B. Dawant, **Surface registration for use in interactive image-guided liver surgery**, in: Proc. MICCAI, volume 1679, 1999, pp. 892–899.

[37] M. A. Audette, T. Peters, **Level-set surface segmentation and registration for computing intrasurgical deformations**, in: Proc. SPIE Med. Img.: Img. Proc., 1999.32

[38] D. M. Cash, M. I. Miga, T. K. Sinha, R. L. Galloway, W. C. Chapman, **Compensating for intraoperative soft-tissue deformations using incomplete surface data and finite elements**, IEEE TMI 24 (2005) 1479–1491.

[39] L. W. Clements, D. M. Cash, W. C. Chapman, R. L. Galloway, M. I. Miga, **Robust surface registration using salient anatomical features in image-guided liver surgery**, in: Proc. SPIE Med. Img.: Vis. Img.-Guided Proc. Disp., 2006.

[40] I. Garg, L. W. Clements, R. L. Galloway, **A computational approach to pre-align point cloud data for surface registration in image guided liver surgery**, in: Proc. SPIE Med. Img.: Vis. Img.-guided Proc., 2007.

[41] D. Cash, M. Miga, S. Glasgow, B. Dawant, L. Clements, Z. Cao, R. Gal- loway, W. Chapman, **Concepts and preliminary data toward the realization of image-guided liver surgery**, J. Gastrointest. Surg. 11 (2007) 844–859.

[42] T. P. Rauth, P. Q. Bao, R. L. Galloway, J. Bieszczad, E. M. Friets, D. A. Knaus, D. B. Kynor, A. J. Herline, **Laparoscopic surface scanning and subsurface targeting: Implications for image-guided laparoscopic liver surgery**, Surgery 142 (2007) 207 – 214.

[43] A. B. Benincasa, C. L. W., H. S. D., G. R. L., **Feasibility study for image-guided kidney surgery: assessment of required intraoperative surface for accurate physical to image space registrations**, Med. Phys. 35 (2008) 4251–4261.

[44] L. W. Clements, W. C. Chapman, B. M. Dawant, R. L. Galloway, M. I. Miga, **Robust surface registration using salient anatomical features for image-guided liver surgery: algorithm and validation**, Med. Phys. 35 (2008) 2528–2540.

[45] P. Dumpuri, L. W. Clements, B. M. Dawant, M. I. Miga, **Model-updated image-guided liver surgery: Preliminary results using surface characterization**, Prog. Biophys. Mol. Bio. 103 (2010) 197 – 207.

[46] D. Rucker, Y. Wu, L. Clements, J. Ondrake, T. Pheiffer, A. Simpson, W. Jarnagin, M. Miga, **A mechanics-based nonrigid registration method for liver surgery using sparse intraoperative data**, IEEE TMI (2013).

[47] D. C. Rucker, Y. Wu, J. E. Ondrake, T. S. Pheiffer, A. L. Simpson, M. I. Miga, **Nonrigid liver registration for image-guided surgery using partial surface data: a novel iterative approach**, in: SPIE Medical Imaging, International Society for Optics and Photonics, 2013, pp. 86710B–86710B.

[48] L. Maier-Hein, P. Mountney, A. Bartoli, H. Elhawary, D. Elson, A. Groch, A. Kolb, M. Rodrigues, J. Sorger, S. Speidel, D. Stoyanov, **Optical techniques for 3D surface reconstruction in computer-assisted laparoscopic surgery**, Med Image Anal 17 (2013) 974–996.

[49] M. Deshmukh, U. Bhosle, **A survey of image registration**, IJIP 5 (2011) 245–269.

[50] A. Sotiras, C. Davatzikos, N. Paragios, **Deformable medical image registration: A survey**, IEEE TMI 32 (2013) 1153 – 1190.

[51] M. A. Audette, F. P. Ferrie, T. M. Peters, **An algorithmic overview of surface registration techniques for medical imaging**, MIA 4 (2000) 201– 217.

[52] J. M. Fitzpatrick, **The role of registration in accurate surgical guidance**, J. Eng. Med. 224 (2010) 607–622.

[53] R. Marmulla, T. Lüth, J. Mühling, S. Hassfeld, **Automated laser registration in image-guided surgery: evaluation of the correlation between laser scan resolution and navigation accuracy**, Int. J. Oral Maxillofac. Surg. 33 (2004) 642–648.

[54] H.-T. Lübbers, F. Matthews, W. Zemann, K. W. Grätz, J. A. Obwegeser, M. Bredell, **Registration for computer-navigated surgery in edentulous patients: A problem-based decision concept**, J. Cranio-Maxillofac. Surg. 39 (2011) 453– 458.

[55] J.-D. Lee, C.-H. Huang, T.-C. Huang, H.-Y. Hsieh, S.-T. Lee, **Medical augment reality using a markerless registration framework**, Exp. Sys. Apps. (2011). In press.

[56] C. Bettschart, A. Kruse, F. Matthews, W. Zemann, J. A. Obwegeser, K. W. Grätz, H.-T. Lübbers, **Point-to-point registration with mandibulo-maxillary splint in open and closed jaw position. evaluation of registration accuracy for computer-aided surgery of the mandible**, J. Cranio- Maxillofac. Surg. (2011). In press.

[57] A. Coffey, M. Miga, I. Chen, R. Thompson, **Toward a preoperative planning tool for brain tumor resection therapies**, Int. J. CARS 8 (2013) 87–97.

[58] D. L. Pham, C. Xu, , J. L. Prince, **Current methods in medical image segmentation**, Annual Review of Biomedical Engineering 2 (2000) 315–337.

[59] O. Wirjadi, **Survey of 3D image segmentation methods**, Technical Report 123, Fraunhofer-Institut für Techno- und Wirtschaftsmathematik, 2007.

[60] T. Heimann, H.-P. Meinzer, **Statistical shape models for 3d medical image segmentation: a review**, Med. Img. Anal. 13 (2009) 543–563.

[61] S. Seitz, B. Curless, J. Diebel, D. Scharstein, R. Szeliski, **A comparison and evaluation of multi-view stereo reconstruction algorithms**, in: Proc. CVPR, 2006.

[62] Y. Furukawa, J. Ponce, **Accurate, dense, and robust multi-view stereopsis**, in: Proc. CVPR, 2007.

[63] J. Salvi, J. Pagès, J. Battle, **Pattern codification strategies in structured light systems**, Patt. Rec. 37 (2004) 827–849.

[64] P. Oberle, **3d laser scanner: Laser surveying, 3d imaging, 3d scanning, lidar**, 2010. URL: http://knol.google.com/k/paul-oberle/ 3d-laser-scanner/13av68kkt1k9q/2.

[65] A. Kolb, E. Barth, R. Koch, R. Larsen, **Time-of-flight sensors in computer graphics**, in: Proc. Eurographics - STAR, 2009, pp. 119–134.

[66] Y. Cui, S. Schuon, C. Derek, S. Thrun, C. Theobalt, **3d shape scanning with a time-of-flight camera**, in: Proc. CVPR, 2010.

[67] S. Mersmann, M. MÄCEller, A. Seitel, F. Arnegger, R. Tetzlaff, J. Dinkel, M. Baumhauer, B. Schmied, H.-P. Meinzer, L. Maier-Hein, **Time-of-flight camera technology for augmented reality in computer-assisted interventions**, in: SPIE Med. Img.: Vis., Img.-Guided Proc., and Mod., 2011.

[68] F. Blais, **Review of 20 years of range sensor development**, J. Elect. Img. 13 (2004) 231–240.

[69] D. Lanman, G. Taubin, **Build your own 3d scanner: 3d photograhy for beginners**, in: ACM SIGGRAPH courses, 2009, pp. 1–87.

[70] A. Groch, A. Seitel, S. Hempel, S. Speidel, R. Engelbrecht, J. Penne, K. Höller, S. Rohl, K. Yung, S. Bodenstedt, F. Pflaum, T. dos Santos, S. Mersmann, H.-P. Meinzer, J. Hornegger, L. Maier-Hein, **3D surface reconstruction for laparoscopic computer-assisted interventions: Comparison of state-of-the-art methods**, in: SPIE Med. Img.: Vis., Img.-Guided Proc., and Mod., 2011.

[71] M.-H. Yang, **Object Recognition**, 2009, pp. 1936–1939.

[72] J. Mundy, **Object recognition in the geometric era: A retrospective**, in: Toward Category-Level Object Recognition, volume 4170, Springer Berlin / Heidelberg, 2006, pp. 3–28.

[73] P. M. Roth, M. Winter, **Survey of Appearance-Based Methods for Object Recognition**, Technical Report, Inst. for Computer Graphics and Vision, Graz University of Technology, Austria, ICG-TR-01/08, 2008.

[74] A. Selinger, **Analysis and Applications of Feature-Based Object Recognition**, Technical Report, Univ. of Rochester. Comp. Sc. Dep., 2001. UR CSD / TR755.

[75] X. J. Li, I. Guskov, **3d object recognition from range images using pyramid matching**, in: Proc. ICCV, 2007, pp. 1–6.

[76] R. B. Rusu, G. Bradski, R. Thibaux, J. Hsu, **Fast 3d recognition and pose using the viewpoint feature histogram**, in: Proc. IEEE IROS, 2010.

[77] R. Detry, J. Piater, **Continuous surface-point distributions for 3d object pose estimation and recognition**, in: Proc. ACCV, 2010, pp. 572–585.

[78] R. Hartley, A. Zisserman, **Multiple View Geometry**, 2 ed., Cambridge Univ. Press, 2003.

[79] C. Hughes, M. Glavin, E. Jones, P. Denny, **Review of geometric distortion compensation in fish-eye cameras**, in: Proc. ISSC, 2008, pp. 162–167.

[80] C. Zhang, Z. Zhang, **Calibration between depth and color sensors for commodity depth cameras**, in: Proc. IEEE ICME, 2011, pp. 1–6.

[81] A. Khodakovsky, P. Alliez, M. Desbrun, P. Schröder, **Near-optimal connectivity encoding of 2-manifold polygon meshes**, Graph. Models 64 (2002) 147–168.

[82] T. Kilgus, T. R. dos Santos, A. Seitel, K. Yung, A. M. Franz, A. Groch, I. Wolf, H.-P. Meinzer, L. Maier-Hein, **Generation of triangle meshes from time-of-flight data for surface registration**, in: Proc. BVM, 2011, pp. 189–193.

[83] B. G. Baumgart, **Winged Edge Polyhedron Representation**, Technical Report, Stanford University, Stanford, CA, USA, 1972. CS-TR-72-320.

[84] B. G. Baumgart, **A polyhedron representation for computer vision**, in: Nat. Comp. Conf., 1975, pp. 589–596.

[85] L. J. Guibas, J. Stolfi, **Primitives for the manipulation of general subdivisions and the computation of voronoi diagrams**, ACM TOG 4 (1985) 74–123.

[86] J. Chen, **Algorithmic graph embeddings**, Theo. Comp. Sc. 181 (1997) 247–266.

[87] E. Akleman, J. Chen, **Guaranteeing the 2-manifold property for meshes with doubly linked face list**, Int. J. Shape Mod. 5 (1999) 149–177.

[88] M. Mäntylä, **Introduction to Solid Modeling**, Computer Science Press, Rockville, Maryland, USA, 1988.

[89] T. R. dos Santos, H.-P. Meinzer, L. Maier-Hein, **Extending the doubly linked face list for the representation of 2-pseudomanifolds and 2-manifolds with boundaries**, Int. J. Comp. Geo. Apps. 21 (2011) 467–494.

[90] M. S. Gockenbach, **Understanding and Implementing the Finite Element Method**, Soc. for Industrial and App. Math., 2006.

[91] R. E. Ong, S. D. Herrell III, M. I. Miga, R. L. Galloway, **A kidney deformation model for use in non-rigid registration during image-guided surgery,** in: Proc. SPIE Med. Img. Vis., Img-Guided Proc., Mod., 2008.

[92] B. Dagon, C. Baur, V. Bettschart, **Real-time update of 3d deformable models for computer aided liver surgery**., in: ICPR, 2008, pp. 1–4.

[93] D.-X. Zhuang, Y.-X. Liu, J.-S. Wu, C.-J. Yao, Y. Mao, C.-X. Zhang, M.-N. Wang, W. Wang, L.-F. Zhou, **A sparse intraoperative data-driven biomechanical model to compensate for brain shift during neuronavigation**, Americ. J. Neurorad. 32 (2010) 395–402.

[94] A. Hostettler, S. Nicolau, C. Forest, L. Soler, Y. Rémond, **Real time simulation of organ motions induced by breathing: First evaluation on patient data**., in: Proc. ISBMS, 2006, pp. 9–18.

[95] D. Aiger, N. J. Mitra, D. Cohen-Or, **4-points congruent sets for robust pairwise surface registration**, ACM TOG 27 (2008) 1–10.

[96] H. Zhang, A. Sheffer, D. Cohen-Or, Q. Zhou, O. van Kaick, A. Tagliasac -chi, **Deformation-driven shape correspondence**, in: Proc. SGP, 2008, pp. 1431–1439.

[97] Y. Zeng, C. Wang, Y. Wang, X. Gu, D. Samaras, N. Paragios, **Dense non-rigid surface registration using high-order graph matching**, in: Proc. CVPR, 2010, pp. 382–389.

[98] P. J. Besl, N. D. McKay, **A method for registration of 3-d shapes**, IEEE TPAMI 14 (1992) 239–256.

[99] I. Eckstein, J.-P. Pons, Y. Tong, C.-C. J. Kuo, M. Desbrun, **Generalized surface flows for mesh processing**, in: Proc. SGP, 2007, pp. 183–192.

[100] C. Papazov, D. Burschka, **Deformable 3d shape registration based on local similarity transforms**, Comp. Graph. Forum 30 (2011) 1493–1502.

[101] J. Shlens, **A Tutorial on Principal Component Analysis**, Technical Report, Institute for Nonlinear Science, UCSD, 2005.

[102] A. M. Bronstein, M. M. Bronstein, R. Kimmel, **Generalized multidimensional scaling: a framework for isometry-invariant partial surface matching**, PNAS 103 (2006) 1168–1172.

[103] Y. Sahillioğlu, Y. Yemez, **Coarse-to-fine combinatorial matching for dense isometric shape correspondence**, Computer Graphics Forum 30 (2011) 1461–1470.

[104] J. Jost, Riemannian **Geometry and Geometric Analysis**, 5 ed., Springer, 2008.

[105] M. Meyer, M. Desbrun, P. Schröder, A. H. Barr, **Discrete differential- geometry operators for triangulated 2-manifolds**, in: Vis. & Math. III, Springer-Verlag, 2003, pp. 35–57.

[106] J. J. Koenderink, A. J. van Doorn, **Surface shape and curvature scales**, Img. & Vis. Comp. 10 (1992) 557–565.

[107] F. Cazals, M. Pouget, **Estimating differential quantities using polynomial fitting of osculating jets**, Comp. Aided Geo. Design 22 (2005) 121–146.

[108] N. Kehtarnavaz, S. Mohan, **A framework for estimation of motion parameters from range image**, Computer Vision, Graphics, and Image Processing 45 (1989) 88–105.

[109] Y. Zeng, C. Wang, Y. Wang, X. Gu, D. Samaras, N. Paragios, **A Generic Local Deformation Model for Shape Registration,** Technical Report RR- 7676, INRIA, 2011.

[110] T. Windheuser, U. Schlickewei, F. R. Schmidt, D. Cremers, **Geometrically consistent elastic matching of 3d shapes: A linear programming solution**, in: Proc. ICCV, 2011.

[111] N. Gelfand, N. J. Mitra, L. J. Guibas, H. Pottmann, **Robust global registration**, in: Proc. SGP, 2005, pp. 197–206.

[112] T. Gatzke, C. Grimm, M. Garland, S. Zelinka, **Curvature maps for local shape comparison**, in: Proc. IEEE Shape Mod. and Apps., 2005, pp. 244–253.

[113] A. E. Johnson, M. Hebert, **Surface matching for object recognition in complex 3-d scenes**, Img. and Vis. Comp. 16 (1998) 635–651.

[114] A. E. Johnson, M. Hebert, **Using spin images for efficient object recognition in cluttered 3d scenes**, IEEE TPAMI 21 (1999) 433–449.

[115] A. Frome, D. Huber, R. Kolluri, T. Bulow, J. Malik, **Recognizing objects in range data using regional point descriptors**, in: Proc. ECCV, 2004.

[116] Y. Sun, M. A. Abidi, **Surface matching by 3d point's fingerprint**, in: Proc.

ICCV, volume 2, 2001, pp. 263–269.

[117] Y. Sun, P. J., A. Koschan, D. L. Page, M. A. Abidi, **Point fingerprint: A new 3-d object representation scheme**, IEEE Trans on Sys., Man, and Cyb. 33 (2003) 712–717.

[118] F. Tombari, S. Salti, L. Di Stefano, **Unique signatures of histograms for local surface description**, in: Proc. ECCV, 2010, pp. 347–360.

[119] F. Tombari, S. Salti, L. Di Stefano, **A combined texture-shape descriptor for enhanced 3d feature matching**, in: Proc. IEEE ICIP, 2011.

[120] T. R. dos Santos, A. Franz, H.-P. Meinzer, L. Maier-Hein, **Robust multi-modal surface matching for intra-operative registration**, in: Proc. IEEE CBMS, 2011.

[121] A. Zaharescu, E. Boyer, K. Varanasi, R. P. Horaud, **Surface feature detection and description with applications to mesh matching**, in: Proc. CVPR, 2009, pp. 373–380.

[122] A. Petrelli, L. Di Stefano, **On the repeatability of the local reference frame for partial shape matching**, in: Proc. ICCV, 2011.

[123] O. K.-C. Au, C.-L. Tai, H.-K. Chu, D. Cohen-Or, T.-Y. Lee, **Skeleton extraction by mesh contraction**, ACM TOG 27 (2008) 44:1–44:10.

[124] X. Zhang, J. Liu, Z. Li, M. Jaeger, **Volume decomposition and hierarchical skeletonization**, in: Proceedings ACM SIGGRAPH VRCAI, 2008, pp. 17:1–17:6.

[125] A. Tagliasacchi, H. Zhang, D. Cohen-Or, **Curve skeleton extraction from incomplete point cloud**, ACM TOG 28 (2009) 71:1–71:9.

[126] J. Cao, A. Tagliasacchi, M. Olson, H. Zhang, Z. Su, **Point cloud skeletons via laplacian based contraction**, in: Proc. IEEE SMI, 2010.

[127] R. Toldo, U. Castellani, A. Fusiello, **Visual vocabulary signature for 3D object retrieval and partial matching**, in: Proc. 3DOR, 2009.

[128] A. M. Bronstein, M. M. Bronstein, L. J. Guibas, M. Ovsjanikov, Shape google: **Geometric words and expressions for invariant shape retrieval**, ACM TOG 30 (2011) 1:1–1:20.

[129] H. Pottmann, J. Wallner, Q.-X. Huang, Y.-L. Yang, **Integral invariants for robust geometry processing**, Comput. Aided Geom. Des. 26 (2009) 37–60.

[130] O. K.-C. Au, C.-L. Tai, D. Cohen-Or, Y. Zheng, H. Fu, **Electors voting for fast automatic shape correspondence**, Comp. Graph. Forum 29 (2010) 645–654.

[131] M. J. Mohlenkamp, **A fast transform for spherical harmonics**, J Fourier Anal. and Apps. 5 (1999) 159–184.

[132] M. Kazhdan, T. Funkhouser, S. Rusinkiewicz, **Rotation invariant spherical harmonic representation of 3d shape descriptors**, in: Proc. SGP, 2003, pp. 156–164.

[133] T. Funkhouser, P. Min, M. Kazhdan, J. Chen, A. Halderman, D. Dobkin, D. Jacobs, **A search engine for 3D models**, ACM TOG 22 (2003) 83–105.

[134] T. Funkhouser, P. Shilane, **Partial matching of 3d shapes with priority-driven search**, in: Proceedings of the fourth Eurographics symposium on Geometry processing, 2006, pp. 131–142.

[135] M. K. Chung, K. M. Dalton, R. J. Davidson, **Encoding neuroanatomical information using weighted spherical harmonic representation**, in: Proc. IEEE SSP, 2007, pp. 146–150.

[136] M. K. Chung, R. Hartley, K. M. Dalton, R. J. Davidson, **Encoding cortical surfaces by spherical harmonics**, Statistica Sinica 18 (2008) 1269–1291.

[137] K. Khairy, J. Howard, **Spherical harmonics-based parametric deconvolution of 3d surface images using bending energy minimization**, Med. Img. Anal. 12 (2008) 217–227.

[138] G. Taubin, **A signal processing approach to fair surface design**, in: Proc.

ACM Comp. Graph. & Interct. Tech., 1995, pp. 351–358.

[139] B. Vallet, B. Lévy, **Spectral geometry processing with manifold harmonics**, in: Proc. EG, 2008, pp. 251–260.

[140] M. Reuter, S. Biasotti, D. Giorgi, G. Patanè, M. Spagnuolo, **Discrete laplace-beltrami operators for shape analysis and segmentation**, Comp. & Grap. 33 (2009) 381–390.

[141] H. Zhang, O. van Kaick, R. Dyer, **Spectral mesh processing**, Comp.

Graph. Forum 29 (2010) 1865–1894.

[142] T. K. Dey, P. Ranjan, Y. Wang, **Convergence, stability, and discrete approximation of laplace spectra**, in: Proc. ACM-SIAM Symp. on Disc. Alg., 2010, pp. 650–663.

[143] A. F. Beardon, **Algebra and Geometry**, 1 ed., Cambridge University, 2005.

[144] H.-Y. Wu, H. Zha, T. Luo, X.-L. Wang, S. Ma, **Global and local isometry-invariant descriptor for 3d shape comparison and partial matching**, in: Proc. CVPR, 2010, pp. 438–445.

[145] M. Reuter, F.-E. Wolter, N. Peinecke, **Laplace-beltrami spectra as "shape-dna" of surfaces and solids**, Comp. Aid. Design 38 (2006) 342–366.

[146] R. M. Rustamov, **Laplace-Beltrami eigenfunctions for deformation invariant shape representation**, in: Proc. SGP, 2007, pp. 225–233.

[147] J. Sun, M. Ovsjanikov, L. Guibas, **A concise and provably informative multi-scale signature based on heat diffusion**, in: Proc. SGP, 2009.

[148] T. K. Dey, K. Li, C. Luo, P. Ranjan, I. Safa, Y. Wang, **Persistent heat signature for pose-oblivious matching of incomplete models**, in: Proc. SGP, 2010.

[149] V. Zobel, J. Reininghaus, I. Hotz, **Generalized heat kernel signatures**, J. WSCG 19 (2011) 93–100.

[150] J. Tangelder, R. Veltkamp, **A survey of content based 3d shape retrieval methods**, in: Proc. IEEE SMI, 2004, pp. 145–156.

[151] B. Bustos, D. A. Keim, D. Saupe, T. Schreck, D. V. Vranić, **Feature-based similarity search in 3d object databases**, ACM Comput. Surv. 37 (2005) 345–387.

[152] N. Iyer, S. Jayanti, K. Lou, Y. Kalyanaraman, K. Ramani, **Three-dimensional shape searching: state-of-the-art review and future trends**, Comput. Aided Des. 37 (2005) 509–530.

[153] A. M. Bronstein, M. M. Bronstein, B. Bustos, U. Castellani, M. Crisani,

B. Falcidieno, L. J. Guibas, I. Kokkinos, V. Murino, M. Ovsjanikov, G. Patané, I. Sipiran, M. Spagnuolo, J. Sun, SHREC 2010: **robust feature detection and description benchmark**, in: Proc. 3DOR, 2010.

[154] P. Heider, A. Pierre-Pierre, R. Li, C. Grimm, **Local shape descriptors, a survey and evaluation**, in: Proc. 3DOR, 2011.

[155] G. Mori, S. Belongie, J. Malik, **Shape contexts enable efficient retrieval of similar shapes**, in: Proc. IEEE CVPR, 2001.

[156] S. M. Yamany, A. A. Farag, **Surfacing signatures: An orientation independent free-form surface representation scheme for the purpose of objects registration and matching**, IEEE TPAMI 24 (2002) 1105–1120.

[157] A. Flint, A. Dick, A. van den Hengel, Thrift: **Local 3d structure recognition**, in: Proc. DICTA, 2007.

[158] C. H. Lee, A. Varshney, D. W. Jacobs, **Mesh saliency**, ACM TOG 24 (2005) 659–666.

[159] R. Gal, D. Cohen-Or, **Salient geometric features for partial shape matching and similarity**, ACM Trans. Graph. 25 (2006) 130–150.

[160] U. Castellani, M. Cristani, S. Fantoni, V. Murino, **Sparse points matching by combining 3d mesh saliency with statistical descriptors**, Comp. Graph. Forum 27 (2008) 643–652.

[161] M. Pauly, R. Keiser, M. Gross, **Multi-scale feature extraction on point-sampled surface**, in: Proc. Eurographics, 2003.

[162] J. Novatnack, K. Nishino, **Scale-dependent 3d geometric features**, in: Proc. IEEE ICCV, 2007.

[163] H. T. Ho, D. Gibbins, **Curvature-based approach for multi-scale feature extraction from 3D meshes and unstructured point clouds**, IET Comput. Vis. 3 (2009) 201–212.

[164] Y. Shan, B. Matei, H. S. Sawhney, R. Kumar, D. Huber, M. Hebert, **Linear model hashing and batch ransac for rapid and accurate object recognition**, in: Proc. IEEE CVPR, 2004, pp. 121–128.

[165] K. Gebal, J. A. Bærentzen, H. Aanæs, R. Larsen, **Shape analysis using the auto diffusion function**, Comp. Graph. Forum 28 (2009) 1405–1413.

[166] C. Weber, S. Hahmann, H. Hagen, **Sharp feature detection in point clouds**, in: Proc. IEEE SMI, 2010, pp. 175–186.

[167] P. Glomb, **Detection of interest points on 3d data: Extending the harris operator**, in: Computer Recognition Systems 3, volume 57 of *Advances in Intelligent and Soft Computing*, Springer, 2009, pp. 103–111.

[168] I. Sipiran, B. Bustos, **A robust 3d interest points detector based on harris operator**., in: Proc. 3DOR, 2010, pp. 7–14.

[169] R. Burkard, M. Dell'Amico, S. Martello, **Assignment Problems**, 1 ed., Society for Industrial and Applied Mathematics, 2009.

[170] S. Sahni, T. Gonzalez, **P-complete approximation problems**, J. ACM 23 (1976) 555–565.

[171] W. Chang, M. Zwicker, **Automatic registration for articulated shapes**, in: Proc. SGP, 2008.

[172] A. Dubrovina, R. Kimmel, **Matching shapes by eigendecomposition of the Laplace-Beltrami operator**, in: Proc. 3DPVT, 2010.

[173] C. Wang, M. M. Bronstein, A. M. Bronstein, N. Paragios, **Discrete minimum distortion correspondence problems for non-rigid shape matching**, in: Proc. SSVM, 2010.

[174] D. Raviv, A. Dubrovina, R. Kimmel, **Hierarchical matching for non-rigid shapes**, in: **Proc**. SSVM, 2011.

[175] Y. Lipman, T. Funkhouser, **Möbius voting for surface correspondence**, ACM TOG 28 (2009) 1–12.

[176] T. R. dos Santos, C. J. Goch, A. M. Franz, H.-P. Meinzer, T. Heimann, L. Maier-Hein, **Minimally deformed correspondences between surfaces for intra-operative registration**, in: Proc. SPIE Med. Img: Img. Proc., 2012.

[177] Y. Lipman, O. Sorkine, D. Levin, D. Cohen-Or, **Linear rotation-invariant coordinates for meshes**, in: Proc. SIGGRAPH, 2005, pp. 479–487.

[178] V. Kraevoy, A. Sheffer, **Mean-value geometry encoding**, Int. J. Shape Mod. 12 (2006) 29–46.

[179] P. G. Ciarlet, **An Introduction to Differential Geometry with Applications to Elasticity**, 1 ed., Springer, 2006.

[180] H. Delingette, **Triangular springs for modeling nonlinear membranes**, IEEE Trans. on Vis. Comp. Graph. 14 (2008) 329–341.

[181] G. Rote, **Computing the minimum hausdorff distance between two point sets on a line under translation**, Inf. Process. Lett. 38 (1991) 123–127.

[182] G. Charpiat, O. Faugeras, R. Keriven, **Approximations of shape metrics and application to shape warping and empirical shape statistics**, Found. Comput.Math.5 (2005) 1–58.

[183] F. Mémoli, **On the use of gromov-hausdorff distances for shape comparison**, in: Proc. EG Symp. on Pto.-based Graph., 2007.

[184] O. van Kaick, H. Zhang, G. Hamarneh, D. Cohen-Or, **A survey on shape correspondence**, in: Proc. EG STAR, 2010.

[185] R. E. Burkard, E. Çela, **Linear assignment problems and extensions**, Handbook of Combinatorial Optimization 4 (1999) 1–54.

[186] M. Dell'Amico, S. Martello, **The k-cardinality assignment problem**, Disc. App. Math. 76 (1997) 103–121.

[187] P. M. Pardalos, F. Rendl, H. Wolkowicz, **The quadratic assignment problem: A survey and recent developments**, in: Proc. DIMACS Work. on QAP, 1994, pp. 1–42.

[188] S. Boyd, L. Vandenbergue, **Convex optimization**, Cambridge Univ. Press, 2006.

[189] E. L. Lawler, D. E. Wood, **Branch-and-bound methods: A survey**, Operations Research 14 (1966) 699–719.

[190] A. J. Stoddart, M. Petrou, J. Kittler, **Probabilistic relaxation as an optimizer**, in: Proc. BMVC, 1995, pp. 613–622.

[191] M. A. Fischler, R. C. Bolles, **Random sample consensus: a paradigm for model fitting with applications to image analysis and automated cartography**, Commun. ACM 24 (1981) 381–395.

[192] A. Tevs, M. Bokeloh, M. Wand, A. Schilling, H.-P. Seidel, **Isometric registration of ambiguous and partial data**., in: Proc. CVPR, 2009, pp. 1185–1192.

[193] I. Borg, P. Groenen, **Modern Multidimensional Scaling: Theory and Applications**, 1 ed., Springer, 1996.

[194] U. Pinkall, S. D. Juni, K. Polthier, **Computing discrete minimal surfaces and their conjugates**, Experimental Mathematics 2 (1993) 15–36.

[195] K. Polthier, **Computational aspects of discrete minimal surfaces**, in: Proc. of the Clay Math. Inst. Summer School, 2005.

[196] J. A. Gallian, **A dynamic survey of graph labeling**, Elect. J. Combinatorics 16 (2009) 1–219.

[197] Y. Boykov, V. Kolmogorov, **An experimental comparison of min-cut/max-flow algorithms for energy minimization in vision**, IEEE TPAMI 26 (2004) 1124–1137.

[198] V. Kolmogorov, C. Rother, **Minimizing nonsubmodular functions with graph cuts - a review**, IEEE TPAMI 29 (2007) 1274–1279.

[199] L. Torresani, V. Kolmogorov, C. Rother, **Feature correspondence via graph matching: Models and global optimization**, in: Proc. ECCV, 2008, pp. 596–609. [200] E. Boros, P. L. Hammer, **Pseudo-boolean optimization**, Disc. App. Math. 123 (2002) 155–225.

[201] H. Ishikawa, **Higher-order clique reduction in binary graph cut**, in: Proc.

IEEE CVPR, 2009, pp. 2993–3000.

[202] T. Werner, **Revisiting the linear programming relaxation approach to gibbs energy minimization and weighted constraint satisfaction**, IEEE TPAMI 32 (2010) 1474–1488.

[203] J. Eckstein, D. P. Bertsekas, **An alternating direction method for linear programming**, Technical Report LIDS-P;1967, Lab. for Inf. and Decision Sys., MIT, 1990.

[204] T. R. dos Santos, A. Seitel, H.-P. Meinzer, L. Maier-Hein, **Correspondences search for surface-based intra-operative registration**, in: Proc. MICCAI, 2010, pp. 660–667.

[205] M. Alexa, D. Cohen-Or, D. Levin, **As-rigid-as-possible shape interpolation**, in: Proc. SIGGRAPH, 2000, pp. 157–164.

[206] R. W. Sumner, J. Popović, **Deformation transfer for triangle meshes**, ACM TOG 23 (2004) 399–405.

[207] T. Igarashi, T. Moscovich, J. F. Hughes, **As-rigid-as-possible shape manipulation**, ACM TOG 24 (2005) 1134–1141.

[208] O. Sorkine, M. Alexa, **As-rigid-as-possible surface modeling**, in: Proc. SGP, 2007, pp. 109–116.

[209] S. Zhang, J. Huang, D. Metaxas, **Robust mesh editing using Laplacian coordinates**, Graph. Models 73 (2011) 10–19.

[210] D. S. Hochbaum, D. B. Shmoys, **A best possible heuristic for the k-center problem**, Math. of Op. Research 10 (1985) 180–184.

[211] A. Sharma, R. Horaud, J. Cech, E. Boyer, **Topologically-robust 3d shape matching based on diffusion geometry and seed growing**, in: Proc. CVPR, 2011.

[212] G. J. McLachlan, T. Krishnan, **The EM Algorithm and Extensions**, Wiley-Interscience, 1996.

[213] S. Kaneko, T. Kondo, A. Miyamoto, **Robust matching of 3D contours using iterative closest point algorithm improved by M-estimation**, Pa 36 (2003) 2041–2047.

[214] M. F. Hansen, M. R. Blas, R. Larsen, **Mahalanobis distance based iterative closest point**, in: Proc. SPIE Med. Img., 2007.

[215] L. Armesto, J. Minguez, L. Montesano, **A generalization of the metric-based iterative closest point technique for 3D scan matching**., in: Proc. ICRA, 2010, pp. 1367–1372.

[216] S. Rusinkiewicz, M. Levoy, **Efficient variants of the ICP algorithm**, in: Proc. 3D Dig. Img. and Mod., 2001.

[217] D. Chetverikov, D. Stepanov, P. Krsek, **Robust euclidean alignment of 3D point sets: the trimmed iterative closest point algorithm**, Img 23 (2005) 299–309.

[218] B. Jian, B. C. Vemuri, **Robust point set registration using gaussian mixture models**, IEEE TPAMI 33 (2011) 1633–1645.

[219] G. P. Penney, P. J. Edwards, A. P. King, J. M. Blackall, P. G. Batchelor, D. J. Hawkes, **A stochastic iterative closest point algorithm (stochastICP)**, in: Proc. MICCAI, 2001, pp. 762–769.

[220] T. Jost, H. Hügli, **A multi-resolution ICP with heuristic closest point search for fast and robust 3D registration of range images**, in: Proc. 3DIM, volume 0, 2003, pp. 427–433.

[221] R. S. J. Estépar, A. Brun, C.-F. Westin, **Robust generalized total least squares iterative closest point registration**, in: Proc. MICCAI, volume 3216, 2004, pp. 234–241.

[222] B. Amberg, S. Romdhani, T. Vetter, **Optimal step nonrigid ICP algorithms for surface registration**, in: Proc. CVPR, 2007.

[223] B. Combès, S. Prima, **Prior affinity measures on matches for ICP-like nonlinear registration of free-form surfaces**, in: Proc. ISBI, 2009, pp. 370–373.

[224] D. Münch, B. Combès, S. Prima, **A modified ICP algorithm for normal-guided surface registration**, in: SPIE Med. Img.: Vis., Img-Guided Proc., volume 7623, 2010.

[225] L. Maier-Hein, A. Franz, T. dos Santos, M. Schmidt, M. Fangerau, H. Meinzer, J. Fitzpatrick, **Convergent iterative closest-point algorithm to accommodate anisotropic and inhomogenous localization error**, IEEE TPAMI 34 (2012) 1520–1532.

[226] L. Oswald, **Recent Development of the Iterative Closest Point Algorithm,** Technical Report, Auton. Sys. Lab., Swiss Federal Institute of Technology, 2010.

[227] B. K. P. Horn, **Closed-form solution of absolute orientation using unit quaternions**, J. Opt. Soc. Am. 4 (1987) 629–642.

[228] J. D. Foley, A. van Dam, S. K. Feiner, J. H. Hughes, **Computer Graphics - Principles and Practice**, 2 ed., Addison-Wesley, Reading, Massachusetts, USA, 1990.

[229] J. Feldmar, N. Ayache, **Rigid, affine and locally affine registration of smooth surfaces**, Technical Report 2220, INRIA, 1994.

[230] F. L. Bookstein, **Principal warps: Thin-plate splines and the decomposition of deformations**, IEEE TPAMI 11 (1989) 567–585.

[231] P. Dierckx, **Curve and Surface Fitting with Splines**, Oxford Univ. Press, 1995.

Data de recebimento: 14/10/2015

Data de aprovação: 15/12/2015

SOBRE O AUTORE

Thiago Ramos dos Santos

Graduado e mestre em Ciências da Computação pela Universidade Federal de Santa Catarina (UFSC), na área de processamento e visualização de imagens médicas, computação gráfica e simulação. Doutorado em Ciências da Computação e Matemática Aplicada pela Universidade de Heidelberg - Alemanha. Foi pesquisador da Div. Medical and Biological Informatics (MBI) do German Cancer Research Center (DKFZ), em Heidelberg - Alemanha, atuando no desenvolvimento de métodos e algoritmos para cirurgia auxiliada por computador e no desenvolvimento da plataforma de software de código-aberto para implementação de aplicações médicas interativas denominada MITK (Medical Imaging and Interaction Toolkit). Atuou como especialista em desenvolvimento industrial na Unidade de Inovação e Tecnologia (UNITEC) do Departamento Nacional do Serviço Nacional de Aprendizagem Industrial (SENAI) / Confederação Nacional da Indústria (CNI), em Brasília - DF. Atualmente cursa MBA em Gestão Financeira pela FGV e atua como diretor do Instituto SENAI de Inovação em Sistemas Embarcados, em Florianópolis - SC.

***